

Four Decades of Research on Thermal Contact, Gap, and Joint Resistance in Microelectronics

M. Michael Yovanovich

Abstract—The Keynote Paper reviews and highlights over 40 years of research on solutions for steady-state and transient thermal constriction and spreading resistances, and thermomechanical models for contact, gap and joint resistances of joints formed by conforming rough surfaces, nonconforming smooth surfaces, and nonconforming rough surfaces. Microgap and macrogap thermal resistance and conductance models are reviewed, and important relations and correlation equations are presented. Contact microhardness, determined by Vickers indenters, are correlated and incorporated into the contact model for conforming rough surfaces. Microhardness parameters are correlated with Brinell hardness values. Elastoplastic contact models for joints formed by smooth sphere-smooth flat and conforming rough surfaces are presented. A simple thermomechanical model for microgaps occupied by oil, grease, grease filled with solid particles, and phase change materials such as paraffins is reviewed, and good agreement with recently published data is noted.

Index Terms—Microgap and macrogap thermal resistance, steady-state, transient thermal constriction, Vickers indenters.

NOMENCLATURE

A_a, A_r	Apparent and real contact areas, m^2 .	d_0	Reference Vickers diagonal, $d_0 = 1 \mu m$.
a	Microcontact spot radius, m.	d_V	Vickers indentation diagonal, μm .
a_1, b_1	Dimensionless correlation coefficients.	E	Young's modulus, GPa.
a'_L	Relative radius of macrocontact, a_L/a_H .	E'	Equivalent elastic modulus, GPa.
a_s	Radius of microcontacts, m.	$\operatorname{erfc}(\cdot)$	Complementary error function.
BGT	Bush, Gibson, and Thomas model.	$\operatorname{erfc}^{-1}(\cdot)$	Inverse complementary error function.
b	Flux tube radius, m.	F	External force, N .
C	Dimensionless constriction resistance parameter for layer-substrate, $C = \psi_{23}/\psi_2$.	F_c	Critical external force, N .
C, C_S, C_F	Joint, solid, fluid conductance, $W/m^2 \cdot K$.	f_g	Microgap gas parameter.
C_c	Dimensionless contact conductance, $C_c = \sigma h_c/mk_s$.	GW	Greenwood and Williamson model.
CLA	Center-line-average surface roughness, μm .	H, H_B	Hardness and bulk hardness, GPa.
C_p	Plastic contact parameter, $C_p = H/S_f$.	H'	Effective microhardness, GPa.
c_1	Vickers microhardness coefficient, GPa.	H_c	Contact microhardness, GPa.
c_2	Vickers microhardness dimensionless coefficient.	H_{BGM}	Geometric mean Brinell hardness, GPa.
c_3	Vickers microhardness coefficient, GPa.	H_L, H_S	Layer and substrate contact microhardness, GPa.
CMY	Cooper, Mikic, and Yovanovich contact conductance model.	H^*	Effective microhardness, $H^* = c_1(\sigma/m\sigma_0)^{c_2}$, GPa.
D	Sphere diameter, m.	h_c, h_g, h_j	Thermal contact, gap and joint conductance, W/m^2K .
d	Vickers indentation depth, μm .	$I_{g,p}$	Dimensionless macrogap gas integral for point contact.
		I_g	Dimensionless microgap gas integral, $I_g = f_g/(Y/\sigma + M/\sigma)$.
		$J_0(\cdot), J_1(\cdot)$	Bessel functions of first kind of order 0 and 1.
		k	Thermal conductivity, W/mK .
		k'	Effective thermal conductivity, W/mK .
		k_s	Harmonic mean thermal conductivity, W/mK .
		L	Sampling length, m.
		L	Elastoconstriction load parameter, $L = D/2a$.
		L	Conforming rough limit length scale, $L = b_L^2/(\sigma/m)$, m.
		\mathcal{L}	Arbitrary length scale, m.
		M	Gas rarefaction parameter, $M = \alpha\beta\Lambda$, m.
		MT	Majumdar and Tien model.
		m	Effective mean absolute surface slope.
		N	Number of microcontacts.
		n	Density of microcontacts, N/A_a .
		P	Contact pressure, MPa.
		P_g	Gas pressure, torr.
		$P_{g,0}$	Reference gas pressure, $P_{g,0} = 760$ torr.
		Pr	Prandtl number, $\mu c_p/k$.
		P^*	Nondimensional pressure, $F/(\pi b_L^2 H^*)$.
		Q	Heat flow rate, W.
		R	Thermal resistance, K/W .
		R_0	Isoflux, constriction/spreading resistance, centroid temperature basis, K/W .
		\bar{R}	Isoflux, constriction/spreading resistance, average temperature basis, K/W .

Manuscript received March 11, 2005; revised April 1, 2005. This work was supported by NSERC and grants and contracts from many Canadian and U.S. nuclear, microelectronics and telecommunications companies and national laboratories. This work was recommended for publication by Associate Editor K. Ramakrishna upon evaluation of the reviewers' comments.

The author is with the Department of Mechanical Engineering, University of Waterloo, Waterloo, ON N2L 3G1, Canada (e-mail: mmyov@mhtlab.uwaterloo.ca).

Digital Object Identifier 10.1109/TCAPT.2005.848483

RMS	Root-mean-square surface roughness.	m	Mean.
$R_{c,i}$	Constriction/spreading resistance of i th microcontact spot, $R_{c,i} = \psi_{c,i}/2k_s a$, K/W.	mac	Macro.
R^*	Dimensionless thermal resistance.	mic	Micro.
S_f	Flow stress, GPa.	p	Plastic contact.
r	Radial coordinate, m.	r	Real.
T	Temperature, K.	s	Small.
T_g	Gas temperature, K.	V	Vickers.
$T_{g,0}$	Reference gas temperature, $T_{g,0} = 288$ K.		
T_m	Mean joint temperature, K.		
TCR	Thermal Contact Resistance, K/W.		
t	Layer thickness or indentation depth, μm .		
WA	Whitehouse and Archard model.		
x	Dimensionless radial position, $x = r/a$.		
Y	Mean surface plane separation, m.		

Greek

α	Accommodation parameter, $(2 - \alpha_1)/\alpha_1 + (2 - \alpha_2)/\alpha_2$.
α_1, α_2	Accommodation coefficients at solid interfaces.
α	Nondimensional parameter, $\sigma\rho/a_H^2$.
β	Dimensionless gas parameter, $2\gamma/(\gamma + 1)Pr$.
β	Radius of curvature of sphere, m.
γ	Ratio of specific heats, c_p/c_v .
δ	Local macrogap thickness, m.
δ_n	Positive roots of $J_1(\delta_n) = 0$.
ϵ_1, ϵ_2	Emissivities of contacting surfaces.
ϵ	Flux tube relative radius $\epsilon = a/b$.
Θ	Nondimensional parameter, R_L/R_s .
κ	Conductivity ratio, k_2/k_3 or k_g/k_s .
Λ	Molecular mean free path, μm .
λ	Relative mean plane separation, Y/σ .
ν	Poisson's ratio.
ρ	Radius of curvature, m.
σ	RMS surface roughness, μm .
σ	Stefan-Boltzmann constant, $\sigma = 5.67 \times 10^{-8} \text{ W/m}^2 \cdot \text{K}^4$.
σ_0	Reference surface roughness, $\sigma_0 = 1 \mu\text{m}$.
τ	Nondimensional parameter ρ/a_H .
ψ	Dimensionless spreading resistance.

Subscripts

1,2	Surface 1,2.
23	Layer-substrate parameter.
a	Apparent.
b	Bulk.
c	Conduction, contact, critical.
e	Effective.
EC	Elastoconstriction.
g	Gap.
GW	Greenwood and Williamson.
H	Hertz.
j	Joint.
L	Large (macro scale).
e	Elastic contact.
ep	Elastoplastic contact.
g	Gap.
j	Joint.

I. INTRODUCTION

THIS Keynote Paper reviews four decades of research on thermal contact, gap, and joint resistances and conductances with applications to microelectronics. It represents a personal journey which began more than 40 years ago and it continues today.

I first heard about thermal contact resistance (TCR) in September 1963 when Professor Warren M. Rohsenow, Massachusetts Institute of Technology (MIT), suggested that I undertake experimental research on TCR as my Ph.D. dissertation. Shortly after accepting Professor Rohsenow's offer, I worked with Professor Henri Fenech, Nuclear Department, MIT, on the experimental program using a novel test rig designed by Dr. J. J. Henry to obtain accurate thermal contact conductance data under vacuum conditions.

During my time at MIT, Professor Michael Cooper of Cambridge University, Cambridge, UK, who was on a sabbatical, and Professor Bora Mikic and I began collaborating on the development of an analytical model for predicting thermal contact conductance of conforming rough surfaces in a vacuum. The geometric-mechanical-thermal model that resulted from this close collaboration was published in 1969, and is called the Cooper-Mikic-Yovanovich (CMY) model. Over the past four decades I have continued working on the CMY model validating its accuracy and extending its applicability to many different types of metals.

After MIT, I joined Professor Henri Cordier's research group in Poitiers, France. During my stay in France, I became aware of other aspects of TCR research such as thermal resistance of joints formed by turned surfaces, effects of thin metallic foils on thermal joint resistance during loading and unloading, etc.

In September 1969, I became an Associate Professor in the Department of Mechanical Engineering, University of Waterloo, Waterloo, ON. I continued my quest for a better understanding of the fundamentals of TCR with financial support from NSERC and the assistance of numerous scholarship graduate students.

The scope of this Keynote Paper precludes presentation of details of all TCR research done from 1963 to the present. Therefore, only the important results will be presented. The review begins with the TCR work done in the U.S. and France in the period from 1966 to 1970. Then the TCR results for the three decades 1970 to 1979, 1980 to 1989, and 1990 to 2005 will be presented.

Three major themes will be considered: i) models for thermal constriction-spreading resistance, ii) models for mechanical contact of conforming rough surfaces and nonconforming smooth surfaces, and iii) models for micro and macrogap resistance and conductance. These themes are closely connected in

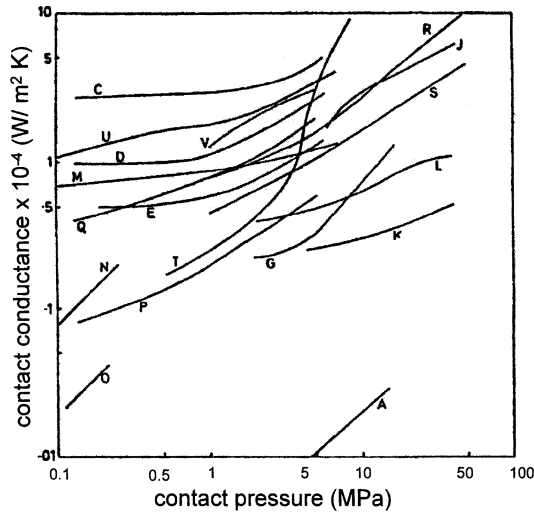


Fig. 3. Contact conductance of copper alloys versus contact pressure.

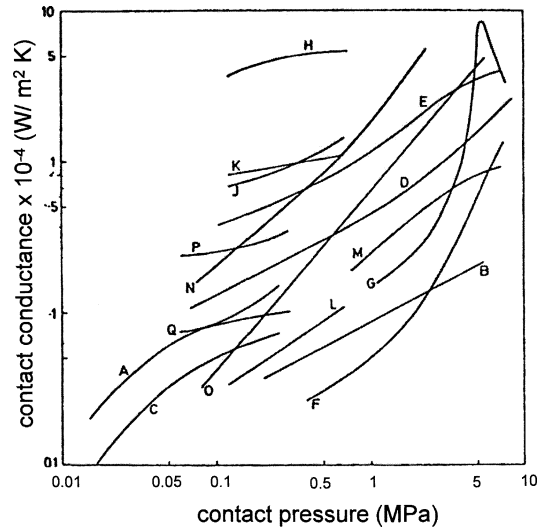


Fig. 6. Contact conductance of miscellaneous materials versus contact pressure.

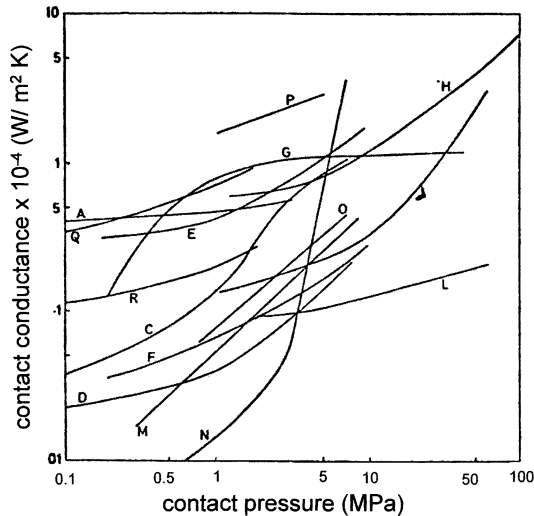


Fig. 4. Contact conductance of stainless steels versus contact pressure.

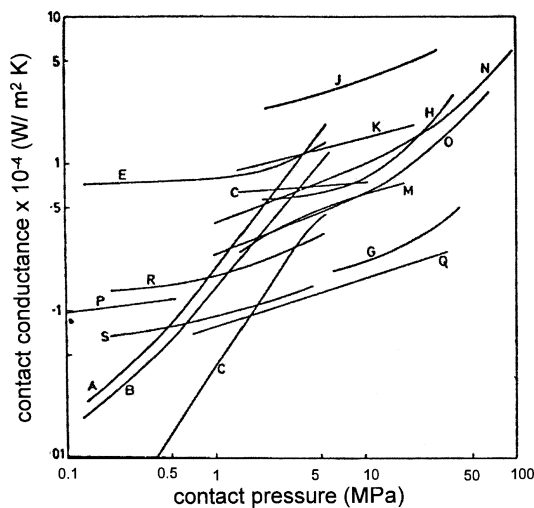


Fig. 5. Contact conductance of other steels versus contact pressure.

several factors such as temperature level, surface roughness and surface out-of-flatness, etc. Fig. 5 shows the effect of contact

pressure on contact conductance for different types of steels. The data were obtained in a vacuum, and other data were obtained with air and other gases such as helium. The trends of C versus P are similar to those reported for the aluminum alloys. Fig. 6 shows the measured contact conductance versus contact pressure for miscellaneous materials.

Thomas and Probert [1] reported that the available simple contact conductance model was expressed as

$$C = C_S + C_F \tag{1}$$

where C , C_S , and C_F are the joint, solid, and fluid conductances, respectively. This simple relation shows that there are two “paths” for the heat to cross the joint: i) by means of the microcontacts and ii) across the microgaps. Radiation heat transfer across the micro and macrogaps was ignored. They concluded from their survey that no satisfactory theory of interface heat transfer exists.

Its apparent that correlations for individual graphs, if they were available, would not be appropriate for the other graphs. Furthermore, correlation equations do not give understanding of the factors which contribute to TCR. In order to develop an accurate joint conductance models, its necessary to conduct basic research at several levels. This systematic approach will be outlined in the following section.

III. TRIAD FOR THERMAL CONTACT RESISTANCE

Before accurate thermal joint conductance (resistance) predictive models can be developed its important to examine the triad for Thermal Contact Resistance which is shown in Fig. 7. The figure shows three basic problems: i) geometry, ii) mechanics, and iii) thermal. The intersection of geometry and mechanics constitutes the contact mechanics problem, the intersection of geometry and thermal constitutes the constriction (spreading) resistance problem, and the intersection of mechanics and thermal constitutes the thermal elastoplasticity problem which will not be discussed in the subsequent sections. The intersection of geometry, mechanics and thermal

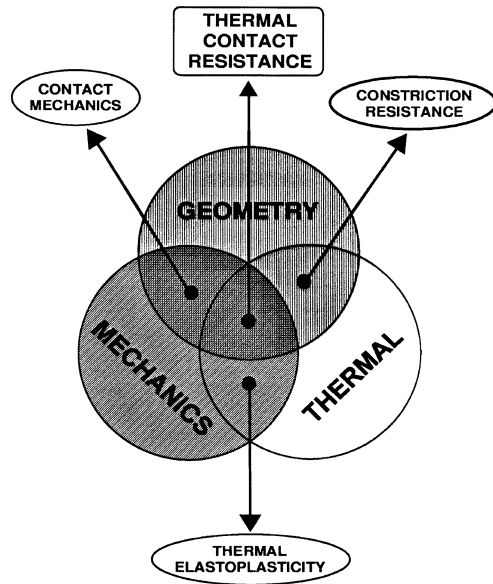


Fig. 7. Triad for thermal contact resistance (conductance).

constitutes the thermal contact resistance problem. For the development of a thermal contact resistance problem, the contact mechanics problem must be solved. There are three types of contact mechanics problems and solutions: a) pure elastic contact, b) pure plastic contact, and c) the more complex elastoplastic contact.

The triad will be used as a guide for the development of different types of geometric-mechanical-thermal contact resistance and conductance models.

Fig. 8 shows several different types of geometric-mechanical joints that can be formed. In all cases shown, the surfaces are assumed to be free of oxides or other contaminants. The surfaces can be smooth and nonconforming as depicted in the left top and bottom joints. The right top and bottom joints show conforming rough surfaces. In the center top and bottom joints are formed by nonconforming and rough surfaces. In the lower row of joints, a uniform thin metallic or nonmetallic layer is bonded to the flat surface called the substrate. This layer influences the mechanical and thermal interaction of the upper and lower surfaces.

The axial force on the joints is assumed to be steady and only the first loading cycle will be considered.

When the surfaces are rough and conforming as shown in the top and bottom right joints, and there is a substance in the microgaps such as air or oil or grease, then microgap resistance-conductance models are required. When the surfaces are smooth and nonconforming as shown in the top and bottom left joints, and the macrogap is occupied with a substance such as air, then a macrogap resistance model is required. For the top and bottom center joints which are formed by rough, nonconforming surfaces, then both micro- and macrogap resistance models are required.

IV. THERMAL CONTACT RESISTANCE RESEARCH 1963–1970

During the first period from 1963 to 1970, the research on TCR was done in the U.S. and France. Several different aspects

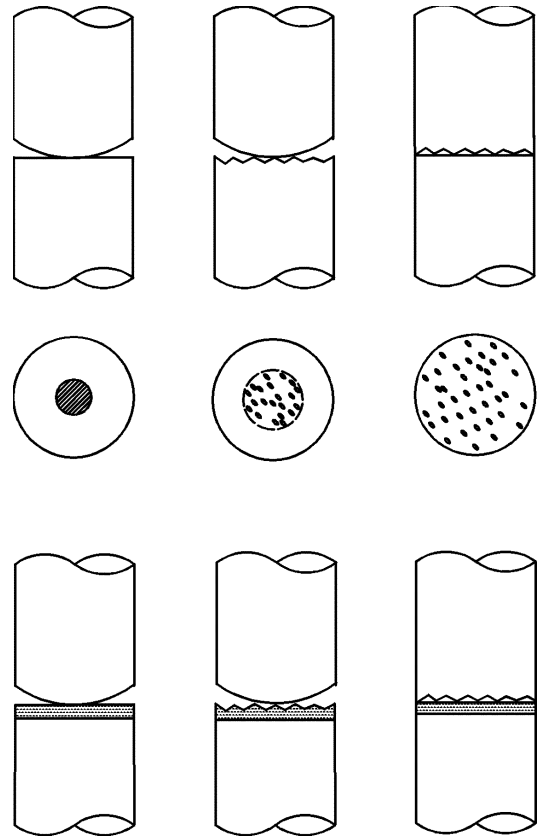


Fig. 8. Schematics of typical mechanical joints.

of thermal contact resistance were examined such as development of models for prediction of thermal contact conductance of joints formed by conforming rough surfaces, a model for thermal resistance of a joint formed by smooth nonconforming surfaces with application to instrument bearings, a model for the thermal joint resistance of nonconforming rough surfaces, a model for the thermal constriction zone, and thermal resistance measurements of soldered joints.

TCR of Nominally Flat Rough Surfaces in a Vacuum. Yovanovich and Fenech [2] examined TCR of nominally flat, rough surfaces in a vacuum both experimentally and analytically. This research showed that the microcontact spots can be modeled as circular areas that separate two “halfspaces” when the joint is in a vacuum. Good agreement was obtained between the data and the TCR model that predicted the number and size of the microcontacts.

Elastoconstriction Resistance Model for Elastically Deformed Spheres in a Vacuum. The elastoconstriction model for TCR across elastically deformed spheres with applications to instrument bearings for spacecraft and satellites was developed [3]. The Hertz theory of elastic contact was used to calculate the circular contact area. The thermal constriction-spreading resistances in the spheres and in the inner race and outer race were modeled as constriction and spreading resistances in half-spaces. A simple gap model for conduction through the gas in the macrogap was presented. This model accounted for slip and rarefaction effects at the gas-solid interfaces. A simple model was proposed for radiative heat transfer in a vacuum or through a transparent gas.

Thermal Constriction Zone. The thermal constriction “zone” was proposed in [4] for steady conduction from an isolated, isothermal circular area into an isotropic halfspace. Oblate spheroidal coordinates were used to obtain an analytical solution which showed that about 98% of the total constriction resistance occurs in a “zone” adjacent to the circular area and that the size of the “zone” is approximately 40 radii. Since a typical microcontact “spot” has a radius of approximately 5–10 μm , the size of the associated constriction “zone” is about 200–400 μm .

Conforming Rough Surface Contact Conductance Model.

The TCR model for conforming (nominally flat) rough surfaces was developed by Cooper, Mikic and Yovanovich [5]. The geometric model is based on the assumptions: the surface asperities have gaussian height distribution about some mean plane of contact and the asperities are distributed randomly over the apparent contact area A_a .

The important surface roughness parameters are the root-mean-square (RMS) roughness or the center-line-average (CLA) roughness which are defined as

$$\left. \begin{aligned} \text{CLA roughness} &= \frac{1}{L} \int_0^L |y(x)| dx \\ \text{RMS roughness} &= \sqrt{\frac{1}{L} \int_0^L y^2(x) dx} \end{aligned} \right\} \quad (2)$$

where $y(x)$ is the distance of points in the surface from the mean plane and L is the length of the trace. The absolute mean asperity slope is defined as

$$m = \frac{1}{L} \int_0^L \left| \frac{dy(x)}{dx} \right| dx. \quad (3)$$

The effective RMS surface roughness and the effective absolute mean asperity slope for a typical joint formed by two conforming rough surfaces are given by [5]

$$\sigma = \sqrt{\sigma_1^2 + \sigma_2^2} \quad \text{and} \quad m = \sqrt{m_1^2 + m_2^2} \quad (4)$$

where σ_1 and σ_2 are the RMS surface roughness and m_1 and m_2 are the mean absolute asperity slope of the contacting surfaces, respectively.

The three deformation models (elastic, plastic, or elastoplastic) give relationships for three important micro-geometric parameters: i) the relative real contact area A_r/A_a , ii) the contact spot density n , and iii) the mean contact spot radius a in terms of the relative mean plane separation defined as $\lambda = Y/\sigma$. The mean plane separation Y and the effective surface roughness are illustrated in Fig. 9 for the joint formed by the mechanical contact of two nominally flat, rough surfaces.

The contact model of the CMY TCR model assumes that one of the contacting surfaces is softer and the deformation is purely plastic whether the harder asperities “penetrate” the softer metal, or whether the softer asperities are “flattened.” There is a contact microhardness H_c that can be assigned to the deformation of the contacting asperities. The overall force balance on the joint yields the following relation:

$$F = PA_a = H_c A_r \quad (5)$$

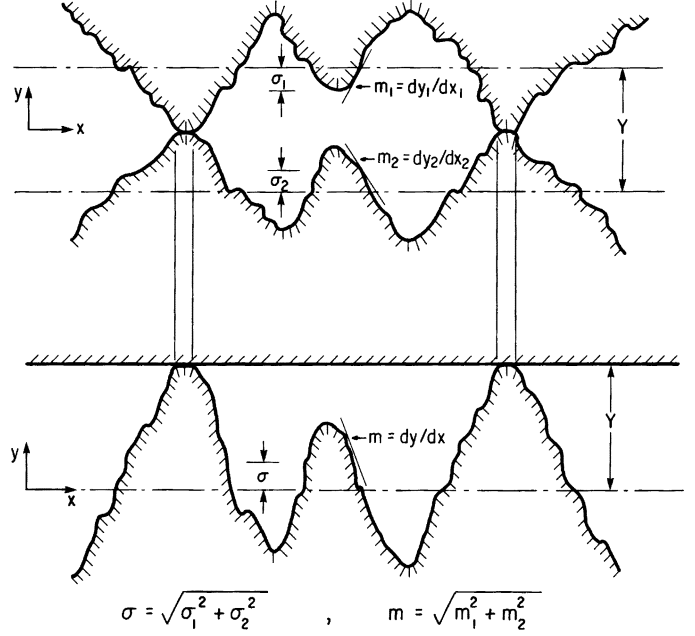


Fig. 9. Typical joint formed by two conforming rough surfaces.

where F is the total force, P is the apparent contact pressure, and A_r and A_a are the total real area and apparent area of contact, respectively. The force balance gives the following relation for the relative real contact in terms of the apparent contact pressure and the microcontact hardness:

$$\frac{A_r}{A_a} = \frac{P}{H_c}. \quad (6)$$

For the plastic deformation model there is one thermal contact conductance model which is given by the relation [5]

$$h_c = \frac{2nak_s}{\psi(\epsilon)} \quad (7)$$

where the effective thermal conductivity of the joint is

$$k_s = \frac{2k_1k_2}{k_1 + k_2}. \quad (8)$$

The thermal constriction parameter ψ , based on isothermal contact spots, is approximated by [5]

$$\psi(\epsilon) = (1 - \epsilon)^{1.5}, \quad \text{for } 0 < \epsilon < 0.3 \quad (9)$$

where the relative contact spot size is $\epsilon = \sqrt{A_r/A_a}$. The geometric parameters n , a and A_r/A_a are related to the relative mean plane separation $\lambda = Y/\sigma$.

Contact Geometric Parameters. For plastic deformation the micro-contact geometric parameters are [5]

$$\left. \begin{aligned} \frac{A_r}{A_a} &= \frac{1}{2} \operatorname{erfc} \left(\frac{\lambda}{\sqrt{2}} \right) \\ n &= \frac{1}{16} \left(\frac{m}{\sigma} \right)^2 \frac{\exp(-\lambda^2)}{\operatorname{erfc} \left(\frac{\lambda}{\sqrt{2}} \right)} \\ a &= \sqrt{\frac{8}{\pi}} \left(\frac{\sigma}{m} \right) \exp \left(\frac{\lambda^2}{2} \right) \operatorname{erfc} \left(\frac{\lambda}{\sqrt{2}} \right) \\ na &= \frac{1}{4\sqrt{2\pi}} \left(\frac{m}{\sigma} \right) \exp \left(-\frac{\lambda^2}{2} \right) \end{aligned} \right\}. \quad (10)$$

Dimensionless Contact Conductance. The dimensionless contact conductance C_c can be expressed in terms of the relative mean plane separation λ [5]

$$C_c \equiv \frac{h_c \sigma}{k_s m} = \frac{1}{2\sqrt{2\pi}} \frac{\exp\left(-\frac{\lambda^2}{2}\right)}{\left[1 - \sqrt{\frac{1}{2}\operatorname{erfc}\left(\frac{\lambda}{\sqrt{2}}\right)}\right]^{1.5}}. \quad (11)$$

This relation is applicable for all mechanical deformation models (elastic, plastic, or elastoplastic).

The correlation equation of the dimensionless contact conductance obtained from theoretical values for a nominal range of λ and P/H_c is [5]

$$C_c \equiv \frac{h_c \sigma}{k_s m} = a_1 \left(\frac{P}{H_c}\right)^{b_1}.$$

The correlation coefficients were given as $a_1 = 1.45$ and $b_1 = 0.985$. The correlation equation was compared with vacuum data for 6 joints formed by stainless steel and aluminum surfaces. The effective surface roughness parameter ranged from $\sigma/m = 12.1 \mu\text{m}$ to $\sigma/m = 85 \mu\text{m}$. The values of the microcontact hardness for the two metals were taken to be $H_c = 2.4 \text{ GPa}$ for the stainless steel joints and $H_c = 0.927 \text{ GPa}$ for the aluminum joints. The data were found to lie in the relative contact pressure range $2 \times 10^{-4} < P/H_c < 3 \times 10^{-2}$. With the exception of several low load points all experimental values of C_c at the higher relative contact pressures fell below the theoretical curve. The data, however, showed loading trends similar to the model predictions.

TCR of Rough, Wavy Surfaces in Vacuum. In paper [6], a theoretical model was presented for the overall thermal contact resistance of a smooth sphere in contact with a rough flat in a vacuum. The radiative heat transfer across the macrogap was assumed to be negligible. The total resistance was based on a simple linear superposition of micro- and macro-constriction resistances. The micro-constriction resistances were based on the CMY model [5].

Thermal Resistance at Soldered Joints. It was shown by several experiments that there is thermal resistance at soldered joints [7]. All tests were performed with nearly identical surface roughness. The measured values ranged from $0.025 \text{ }^\circ\text{C} \cdot \text{cm}^2/\text{W}$ for the “best” joint (brass/brass) to $0.14 \text{ }^\circ\text{C} \cdot \text{cm}^2/\text{W}$ for a poorly soldered joint. The variation in the values was consistent with the quality of the solder. The measured values were much greater than the theoretical value of $0.00246 \text{ }^\circ\text{C} \cdot \text{cm}^2/\text{W}$ for an average solder thickness of $15 \mu\text{m}$ and an effective surface roughness of about $0.5 \mu\text{m}$. Correlations were presented in [8].

V. THERMAL CONTACT RESISTANCE RESEARCH 1970–1980

The research accomplished in the period 1970–1980 consisted of many analytical and numerical studies, and several experimental investigations on constriction and spreading resistances, development and experimental validation of elastoconstriction and elastogap resistance models, and measurement of the effect of metallic foils on TCR and development of correlation equations for the optimum foil thickness, and other investigations [10], [12], [15], [18].

Constriction-Spreading Resistances. The analytical studies of steady and transient constriction and spreading resistances in isotropic halfspaces and flux tubes and channels are given in references [16], [19]–[25], and [29]. The effects of shape, boundary conditions, and the length scale on constriction-spreading resistances were examined. It was found that the dimensionless spreading resistance defined as

$$k\mathcal{L}R_s \quad (12)$$

where R_s is the spreading resistance, k is the thermal conductivity of the halfspace (substrate), and \mathcal{L} is the arbitrary length scale of the source area depends on boundary condition (e.g., isoflux, isothermal) and the shape of the source area.

For the circular and elliptical geometries the isoflux condition results in a spreading resistance which is about 8% greater than the isothermal condition. This relatively small difference was observed for other geometries such as regular polygonal areas, semicircles, etc. If the arbitrary length scale is chosen to be $\mathcal{L} = \sqrt{A}$, where A is the area of the source, the effects of shape and aspect ratio become negligible. Thus, the constriction and spreading resistances of rectangular and elliptical source areas having identical boundary conditions, area, and aspect ratio are very close in value. All numerical values of the dimensionless spreading resistances for singly-connected sources lie in the following narrow ranges: see (13), shown at the bottom of the page. For the isoflux sources useful approximations are $k\sqrt{A}R_0 = 5/9$ and $k\sqrt{A}R = 0.84k\sqrt{A}R_0$. For isothermal sources a useful approximation is $k\sqrt{A}R = 4/9$.

It was also found by numerical studies that the dimensionless spreading resistances of doubly-connected source areas such as regular polygonal areas having identical source areas $A_c = A_o - A_i$, aspect ratios $\sqrt{A_i}/A_o$, and identical boundary conditions, have similar dimensionless resistances defined as

$$k\sqrt{A_c}R_s \quad (14)$$

where A_c is the total source area and A_i and A_o are the inner and outer areas. Correlation equations were developed. The solutions and correlation equations are summarized in Chapter 4 of the *Handbook of Heat Transfer* [105].

$$\left. \begin{array}{l} 0.5197 \leq k\sqrt{A}R_0 \leq 0.5616 \\ 0.4424 \leq k\sqrt{A}R \leq 0.4733 \\ 0.4380 \leq k\sqrt{A}R \leq 0.4432 \end{array} \right\} \begin{array}{l} \text{isoflux, centroid temperature basis} \\ \text{isoflux, average temperature basis} \\ \text{isothermal} \end{array} \quad (13)$$

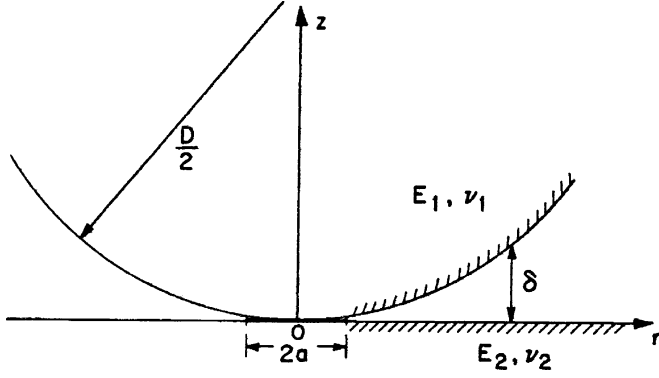


Fig. 10. Schematic of sphere-flat contact and macrogap.

 TABLE I
 TEST PARAMETER VALUES FOR SPHERE-FLAT CONTACT

$D = 25.4 \text{ mm}$	$\epsilon_1 = 0.2$	$k_1 = 50.2 \text{ W/m} \cdot \text{K}$
$P_g = 10^{-6} \text{ torr}$	$\epsilon_2 = 0.8$	$k_2 = 52.8 \text{ W/m} \cdot \text{K}$
$E_1 = 206 \text{ GPa}$	$\nu_1 = 0.3$	$k_s = 51.5 \text{ W/m} \cdot \text{K}$
$E_2 = 206 \text{ GPa}$	$\nu_2 = 0.3$	

Elastoconstriction and Elastogap Resistance Models. Seven publications deal with analytical models [9], [11], [14], [27] and experimental investigations [17], [28] of elastoconstriction and elastogap resistances. The elastoconstriction resistance models [9], [11], [14], [26], [27], and the experiments of elastogap resistance of a sphere-flat contact [17] in a vacuum, and with air and argon in the macrogaps. Hertz elastic contact theory was used to predict the radius of contact for the elastoconstriction resistance, and the local gap thickness for the elastogap resistance.

The elastic contact of a smooth sphere of radius $D/2$ and a smooth flat is shown in Fig. 10. The contact radius is a , and the local macrogap thickness is δ . The elastic properties of the sphere and flat, respectively, are E_1, ν_1 and E_2, ν_2 . The mechanical and thermal models are given in [14] and the experiments and test results are given in [17]. The elastoconstriction model with radiative heat transfer and the vacuum test results are compared in Table I.

The test parameter values are listed in Table I.

Dimensionless Contact Resistance. The dimensionless contact resistance is defined as $R_c^* = Dk_s R_c$. Its given by the following relation:

$$R_c^* = L \left(1 - \frac{1}{L} \right)^{1.5} \quad (15)$$

where the elastic load parameter is obtained from the Hertz theory [9], [14]

$$\frac{1}{L} = \left[\frac{3F}{D^2} \left(\frac{1 - \nu_1^2}{E_1} + \frac{1 - \nu_2^2}{E_2} \right) \right]^{\frac{1}{3}} \quad (16)$$

where F is the the external force on the contact, and also $L = D/2a$.

 TABLE II
 COMPARISONS OF ELASTOCONSTRICTION RESISTANCE MODEL AND VACUUM DATA

L	T_m K	R_c^*	R_r^*	R_j^* model	R_j^* tests	% diff.
179.5	337.0	178.0	1398	157.9	163.3	3.31
115.1	321.0	113.6	1618	106.1	107.0	0.84
103.2	321.0	101.7	1618	95.7	99.4	3.73
89.6	328.0	88.1	1517	83.3	83.2	-0.07
76.0	321.0	74.5	1618	71.2	70.9	-0.45
65.4	320.0	63.9	1633	61.5	61.9	0.65
50.0	319.0	48.5	1649	47.1	48.8	3.44
45.0	318.0	43.5	1664	42.4	42.6	0.47
37.4	316.0	35.9	1696	35.8	35.4	0.65

Dimensionless Radiation Resistance. The dimensionless radiation resistance is defined as $R_r^* = Dk_s R_r$. The dimensionless radiation resistance for the complex enclosure formed by the sphere-flat contact and the surrounding insulation is given by the following relation [14]:

$$R_r^* = \frac{k_s}{\pi D \sigma T_m^3} \left[0.577 + \frac{1 - \epsilon_2}{2\epsilon_2} + \frac{1 - \epsilon_1}{\epsilon_1} \right] \quad (17)$$

where D is the sphere diameter, $\sigma = 5.67 \times 10^{-8} \text{ W/m}^2 \cdot \text{K}^4$ is the Stefan-Boltzmann constant, $T_m = (T_1 + T_2)/2$ is the absolute temperature of the sphere-flat gap, and T_1 and T_2 are the extrapolated absolute temperatures of the sphere and flat respectively. Also, ϵ_1 and ϵ_2 are the emissivities of the sphere and flat, respectively. For the system the dimensionless radiation resistance can be expressed as

$$R_r^* = 1982 \left(\frac{300}{T_m} \right)^3. \quad (18)$$

Dimensionless Joint Resistance. The dimensionless joint resistance is defined as $R_j^* = Dk_s R_j$. According to the decoupled model, the dimensionless joint resistance depends on the contact and radiation resistances in the following manner:

$$\frac{1}{R_j^*} = \frac{1}{R_c^*} + \frac{1}{R_r^*}. \quad (19)$$

The model predictions [14] and the experimental data [17] are compared in Table III for a range of loads. Since the values of T_m were in a relatively narrow range: $316 \text{ K} \leq T_m \leq 337 \text{ K}$, the values of the dimensionless radiation resistance were also in a narrow range: $1398 \leq R_r^* \leq 1696$. The dimensionless radiation resistance values for all loads were greater than the values of the dimensionless contact resistance which varied with the load.

The agreement between the predicted values of the elastoconstriction model and the experimental values as given in Table II is excellent for all dimensionless loads L . The maximum percent difference is about 3.7%, and the RMS percent difference is approximately 2.2%.

Elastogap Resistance. The elastogap resistance model is based on a coupled temperature [14]. Its given by

$$R_g = \frac{L^2}{k_g D I_{g,p}} \quad (20)$$

TABLE III
ELASTOGAP RESISTANCE THEORY AND MEASUREMENTS FOR
 $D = 25.4$ mm, $L = 115.1$, AND AIR

T_m K	P_g torr	R_g^* Model	R_r^* Model	R_j^* Theory	R_j^* Test
309	400.0	76.9	1293	44.5	46.8
310	100.0	87.4	1280	47.8	49.6
311	40.0	97.1	1268	50.6	52.3
316	4.4	137.2	1209	59.5	59.0
318	1.8	167.2	1186	64.5	65.7
321	0.6	227.9	1153	71.7	73.1
322	0.5	246.6	1143	73.4	74.3
325	0.2	345.4	1111	80.1	80.3
321	vacuum	∞	1155	104.7	107.0

where the elastogap integral is defined as

$$I_{g,p} = \int_1^L \frac{2x \tan^{-1} \sqrt{x^2 - 1}}{\frac{2\delta}{D} + \frac{2M}{D}} dx \quad (21)$$

where $x = r/a$.

The macrogap resistance integral depends on two dimensionless geometric parameters: $2\delta/D$ and $2M/D$. The dimensionless local gap thickness in the interval $1 \leq x \leq L$ where $x = r/a$ is [14]

$$\frac{2\delta}{D} = 1 - \left[1 - \left(\frac{x}{L} \right)^2 \right]^{\frac{1}{2}} + \frac{1}{\pi L^2} \left[(2 - x^2) \sin^{-1} \left(\frac{1}{x} \right) + \sqrt{x^2 - 1} \right] - \frac{1}{L^2}. \quad (22)$$

The dimensionless gas rarefaction parameter is

$$\frac{M}{D} = \frac{\alpha\beta\Lambda}{D} \quad (23)$$

with

$$\left. \begin{aligned} \alpha &= \frac{2-\alpha_1}{\alpha_1} + \frac{2-\alpha_2}{\alpha_2} \\ \beta &= \frac{2\gamma}{(\gamma+1)Pr} \\ \Lambda &= \Lambda_0 \left(\frac{T_g}{T_{g,0}} \right) \left(\frac{P_{g,0}}{P_g} \right) \end{aligned} \right\} \quad (24)$$

where α is the accommodation parameter and α_1, α_2 are the thermal accommodation coefficients at the gas-sphere and gas-flat interfaces, respectively. The gas parameter β depends on the ratio of the specific heats $\gamma = c_p/c_v$, and the Prandtl number Pr . The molecular mean free path of the gas Λ is related to the reference value Λ_0 at reference temperature $T_{g,0}$ and reference gas pressure $P_{g,0}$, and the gap gas temperature T_g and gas pressure P_g . For the smooth sphere and smooth flat joint, with air in the macrogap, $\Lambda_0 = 64$ nm at $T_{g,0} = 288$ K and $P_{g,0} = 760$ torr, $\gamma = 1.61$, $Pr = 0.70$, and $\alpha_1 = 0.80$, $\alpha_2 = 0.85$.

For these tests the dimensionless radiation resistance of the sphere-flat-insulation enclosure for the system parameters is

$$R_r^* = 1982 \left(\frac{300}{T_m} \right)^3. \quad (25)$$

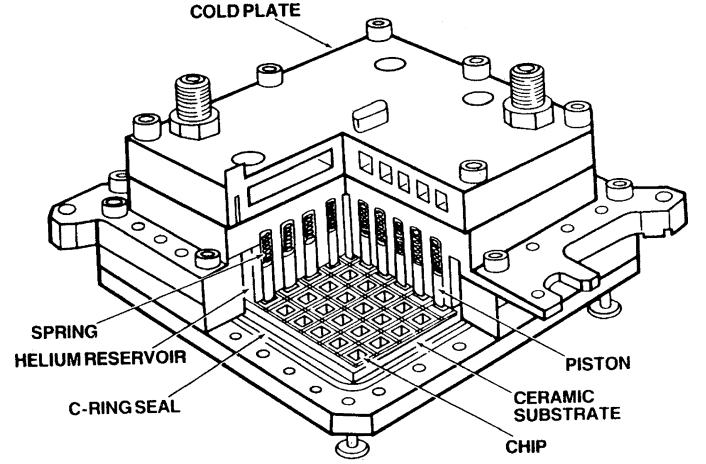


Fig. 11. IBM thermal conduction module (TCM).

The comparison between the predictions of the elastoconstriction and elastogap models and the experimental data for the fixed load $L = 115.1$ and gas pressures ranging from 400 torr to a vacuum are given in Table III. The agreement between the theoretical models and the data is excellent for all test points.

The largest difference occurs at the highest gas pressures where the theory predicts lower joint resistances by approximately 5%. The agreement between theory and experiment improves with decreasing gas pressure.

It is also shown in Table III, that the presence of air in the sphere-flat macrogap significantly decreases the joint resistance when compared with the vacuum results. The elastogap model can be used to predict the performance of other gases such as argon and helium.

The IBM thermal conduction module (TCM) shown in Fig. 11 is an excellent example of the application of the elastogap resistance model (EGR) to an important microelectronics system. In the TCM aluminum pistons with smooth hemispherical ends were spring loaded to make light contact with the chips. The macrogap was filled with helium. This system removed the heat generated by the devices, and it was carried away by water cooled cold plates.

Effect of Metallic Foils on TCR: Optimum Foil Thickness.

An experimental investigation on the effect of metallic foils on TCR of a turned surface in contact with an optically flat surface in air [13] showed that there is an optimum thickness. Test results are shown in Figs. 12 and 13 for tin and lead foils, respectively. Similar results were obtained with aluminum and copper foils for loading and unloading tests. A minimum joint resistance was observed in all tests.

The nominal values of the physical and thermal properties of the metallic foils used to determine the optimum thickness are listed in Table IV.

The foil thickness was varied from 10 to 500 μm . The tests with foils followed the thickness sequence: 500, 100, 50, 25, and 10 μm . The last test was the bare surface test. All tests were conducted in air at 1 atm. The forces on the joint were 20, 40, 60, 80, and 100 kg/cm^2 . The joint was formed by the contact of a turned surface and an optically flat surface. The lathe turned surface had the following characteristics: sawtooth peak-to-valley

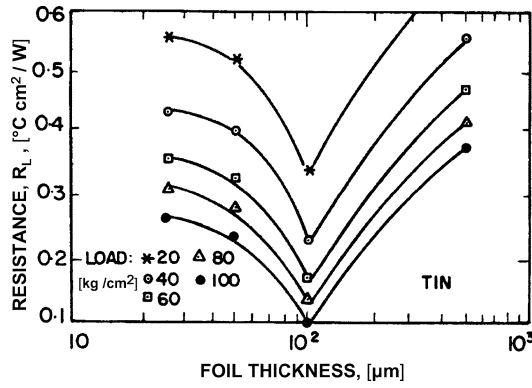


Fig. 12. Effect of tin foil thickness during first load.

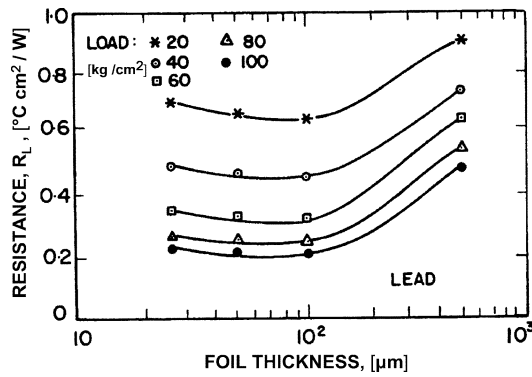


Fig. 13. Effect of lead foil thickness during first load.

TABLE IV
HARDNESS AND CONDUCTIVITY OF METALLIC FOILS

Metal Foil	Foil Hardness H_f , kg/mm ²	Foil Conductivity k_f , W/m K
Lead	4.0	35
Tin	5.3	60
Aluminum	27	204
Copper	80	384

height was 90 μm and the peak-to-peak span was 180 μm. The RMS roughness was measured with a profilometer and found to be approximately 52 μm. The bare turned and optically flat surfaces were armco iron.

The test results for loading and unloading showed a minimum joint resistance for a particular foil thickness. All metallic foils showed a significant reduction in the joint resistance with respect to the bare joint resistance. The ratios of the joint resistance with metallic foil divided by the joint resistance of the bare joint for all foils and all loads are tabulated in Table V.

A correlation equation was developed for the resistance ratio for the first load tests only

$$R^* = \frac{R(\text{minimum resistance})}{R(\text{bare surface})} \quad (26)$$

It is

$$R^* = \frac{1}{\exp\left(0.0072P + 15.5\left(\frac{k_f}{H_f}\right)^{0.92}\right)} \quad (27)$$

TABLE V
RATIO OF MINIMUM JOINT RESISTANCE WITH FOIL TO BARE SURFACE

P (kg/cm ²)	20	40	60	80	100
Metallic Foil					
Tin	0.082	0.071	0.063	0.055	0.046
Lead	0.163	0.139	0.116	0.088	0.064
Aluminum	0.204	0.195	0.182	0.167	0.145
Copper	0.324	0.284	0.254	0.218	0.182

The units of the parameters that appear in the correlation equation are P (kg/cm²), k_f (W/cm²°C), and H_f (kg/mm²) [30], [33].

VI. THERMAL CONTACT RESISTANCE RESEARCH 1980–1990

Several different aspects of TCR were studied in this decade. Many publications dealt with steady and transient constriction [39], [43], [52] and spreading resistances in a halfspace [37], [40], [42], [47], [49], [50], [65], [66], [67], and in flux tubes [46], [47], [49], [50], [59], [62], [69], [70] and channels [41], [45]. Experiments were conducted on the microhardness variation due to workhardening [32], [35], [64]. The effect of oxides [34] and thin metallic layers on TCR were examined experimentally [34], [38], [44], [54], [68], [72] and analytically [44], [52], [54], [57], [58], [61]. A model was developed for a bolted joint [55] for microelectronic applications. Most of the research effort on TCR was directed toward microelectronic issues and a couple were directed to nuclear issues [34], [53]. Special topics [36], [41], [45], [48], [51], [56][58], [60], [61], [70], [74], [77] were studied.

Model development and experiments were directed to a better understanding of heat transfer across the microgaps formed by conforming rough surfaces [31], [54], [63], [71] for microelectronic and nuclear applications. The work on TCR done prior to 1986 was summarized and given in keynote papers [59], [64], and in a book chapter [67].

Three important topics will be given in this section: i) the microhardness variation due to workhardening, ii) the microgap conductance model and correlations, and iii) the model and experiments for the effect of a softer, higher thermal conductivity layer bonded to a substrate.

Extended Conforming Rough Surface Model. The conforming rough surface model of [5] was re-examined in 1981 [31] and a new, more accurate, correlation equation was proposed for the contact conductance h_c

$$C_c = \frac{\sigma h_c}{m k_s} = 1.25 \left(\frac{P}{H_c}\right)^{0.95} \quad (28)$$

This correlation equation of the theoretical values is accurate to ±1.5% in the range: $2 \leq \lambda = Y/\sigma \leq 4.75$. Since the relative mean plane separation λ and the relative contact pressure P/H_c are related as

$$\lambda = \sqrt{2} \operatorname{erfc}^{-1} \left(\frac{2P}{H_c}\right) \quad (29)$$

The correlation equation is applicable in the range: $10^{-6} \leq P/H_c \leq 2.2 \times 10^{-2}$.

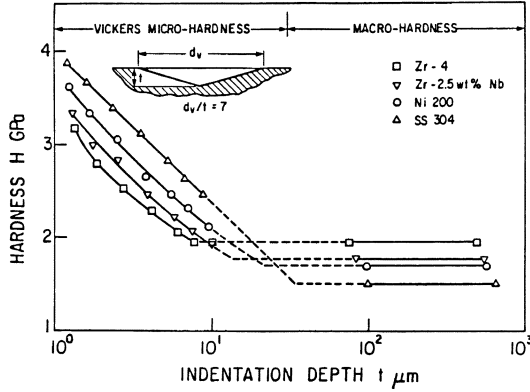


Fig. 14. Vickers microhardness, and Brinell and Rockwell C hardness values.

Vickers microhardness measurements on ground, lapped and polished Ni 200, SS 304, and two zirconium alloys revealed the thin microhardness layer as shown in Fig. 14. The Brinell and Rockwell C hardness values are also shown in Fig. 14. The microhardness and hardness (bulk) values are plotted with respect to the indentation depth t . The mean Vickers diagonal d_V and the depth of penetration are related as $d_V = 7t$. The Vickers indentation depths are in the range from about $1 \mu\text{m}$ to values below about $10 \mu\text{m}$. The Rockwell C indentation depths lie just below $100 \mu\text{m}$, and the Brinell indentations are the largest and they fall in the 700 to $900 \mu\text{m}$ range.

The Vickers microhardness measurements were correlated with respect to the depth of indentation and the Vickers mean diagonal. The Vickers indentation depth was used initially [32], [35], and correlations equations were found having the form

$$H_V(\text{kg/mm}^2) = c_1 t^{c_2} + c_3. \quad (30)$$

For the Ni 200 Vickers measurements the maximum value $H_V = 362.3 \text{ kg/mm}^2$ corresponds to the smallest depth of penetration $t = 1.24 \mu\text{m}$. The minimum value of the hardness was determined by Brinell and Rockwell C testers to be $H_b = 170.4 \text{ kg/mm}^2$. The depth of penetration is determined by extrapolation of the Vickers correlation equation which gives $t_b = 21.56 \mu\text{m}$ when $H_V = 170.4 \text{ kg/mm}^2$. The correlation coefficients for the Ni 200 surface are

$$c_1 = 377.27 \text{ kg/mm}^2 \quad c_2 = -0.274 \quad c_3 = 7.79 \text{ kg/mm}^2. \quad (31)$$

The correlation equation gives the following values:

$$\left. \begin{aligned} H_V(t = 1.24 \mu\text{m}) &= 363.5 \text{ kg/mm}^2 \\ H_V(t = 10.00 \mu\text{m}) &= 208.5 \text{ kg/mm}^2 \\ H_V(t = 21.56 \mu\text{m}) &= 170.4 \text{ kg/mm}^2 \end{aligned} \right\}. \quad (32)$$

SS 304 Correlation Coefficients. The Vickers microhardness measurements were correlated and the correlation coefficients are

$$c_1 = 3047 \text{ kg/mm}^2 \quad c_2 = -0.024 \quad c_3 = -2650 \text{ kg/mm}^2. \quad (33)$$

The correlation equation gives the following values:

$$\left. \begin{aligned} H_V(t = 1.20 \mu\text{m}) &= 383.7 \text{ kg/mm}^2 \\ H_V(t = 10.00 \mu\text{m}) &= 233.2 \text{ kg/mm}^2 \\ H_V(t = 21.56 \mu\text{m}) &= 149.7 \text{ kg/mm}^2 \end{aligned} \right\}. \quad (34)$$

The Brinell and Rockwell C indentation tests gave identical values for the bulk hardness: $H_b = 150 \text{ kg/mm}^2$. The penetration depths were approximately $100 \mu\text{m}$ for the Rockwell indentation and $700 \mu\text{m}$ for the Brinell indentation.

Contact Microhardness Correlation Equation. An approximate contact microhardness model and correlation equation was developed for the Ni 200 and SS 304 metals. In the model it is assumed that the average microcontact spot area $A_c = \pi a^2$ is equivalent to the Vickers projected area $A_V = d_V^2/2$. If the Vickers diagonal is replaced by the depth of penetration we have $A_V = 49t^2/2$. The depth of penetration is related to the mean contact spot radius

$$t = \left(\frac{\pi a^2}{24.5} \right)^{\frac{1}{2}} = 0.358a. \quad (35)$$

The contact microhardness is obtained from

$$H_c = H_V(t) = c_1(0.358a)^{c_2} + c_3 \quad (36)$$

if the mean contact spot is known. In the next step, in the development of a correlation equation we use the approximation for the mean contact spot radius

$$a = 0.99 \left(\frac{\sigma}{m} \right) \left[-\ln \left(\frac{3.132P}{H_b} \right) \right]^{-0.547} \quad (37)$$

where the units of σ/m are microns. This relation shows how the mean contact spot radius depends on the effective surface roughness σ/m and the relative contact pressure P/H_b . After substitution for a and putting $\sigma \times 10^6/m$, we obtain the correlation equation for the contact microhardness of Ni 200 surfaces

$$H_c(\text{kg/mm}^2) = 11.38 \left(\frac{m}{\sigma} \right)^{0.274} \left[-\ln \left(\frac{3.132P}{H_b} \right) \right]^{0.150} + 7.79. \quad (38)$$

The units of σ are μm , and the units of P and H_b must be consistent. The correlation equation shows that the contact microhardness decreases with increasing surface roughness and contact pressure.

Alternative power-law correlation equations were developed based on the mean Vickers diagonal [35], [63]. Its given by

$$H_V = c_1 \left(\frac{d_V}{d_0} \right)^{c_2}, \quad \text{where } d_0 = 1 \mu\text{m} \quad (39)$$

where H_V is the Vickers microhardness, and c_1 and c_2 are the correlation coefficients. The Vickers microhardness correlation coefficients c_1 , c_2 , the maximum and RMS percent differences, and the bulk hardness H_b determined by the Brinell and Rockwell C hardness indentations are given in Table VI.

The ratio of the largest and smallest values of H_b , c_1 and c_2 are 1.30, 1.11, and 1.21, respectively.

TABLE VI
VICKERS MICROHARDNESS CORRELATION COEFFICIENTS

Metal	H_b , GPa	c_1 , GPa	c_2	Max% Diff.	RMS% Diff.
Ni200	1.668	6.30	-0.264	4.8	1.8
SS304	1.472	6.27	-0.229	4.2	1.4
Zr-4	1.913	5.68	-0.278	3.4	1.7
Zr-2.5wt%Nb	1.727	5.88	-0.267	10.2	2.7

For the four metals the bulk hardness H_m as determined by Brinell and Rockwell C hardness testers, the bulk hardness was in the narrow range: $1.472 \leq H_m \leq 1.913$. It was found that the average value of the index is $c_2 = -0.26$. The correlation coefficient was closely related to the bulk hardness as [35], [63]

$$c_1 = 12.04 - 3.49H_m \quad \text{GPa.} \quad (40)$$

All Vickers microhardness measurements for the four metals were accurately correlated by

$$H_v = (12.04 - 3.49H_m) \left(\frac{d_V}{d_0} \right)^{-0.26}. \quad (41)$$

Several models [32], [35] were proposed to calculate the appropriate value of H_c given the effective interface roughness σ/m and the contact pressure. The most accurate model required an iterative method, and two approximate methods were proposed. In [63] an explicit relation was found for the relative contact pressure

$$\frac{P}{H_c} = \left[\frac{P}{(1.62 \times 10^6 \sigma/m)^{c_2}} \right]^{\frac{1}{(1+0.071c_2)}}. \quad (42)$$

This relation shows how the relative contact pressure depends on the contact pressure, the effective interface roughness, and the Vickers microhardness correlation coefficients. Therefore the effective microhardness H_c depends on σ/m , the Vickers correlation coefficients and the contact pressure.

The vacuum test results for the four metals are compared with the extended CMY model in Fig. 15 where the values of the dimensionless contact conductance $(\sigma/m)(h_c/k_s)$ are plotted against the relative contact pressure defined as P/H_e where H_e was called the "effective" contact microhardness.

All data fall in the range: $10^{-4} \leq P/H_e \leq 10^{-2}$. The extended CMY model appears as the straight line corresponding to the relation $(\sigma/m)(h_c/k_s) = 1.25 (P/H_e)^{0.95}$ which is based on the theoretical values.

The values of σ and m for the four metals are listed in the legend. The bulk hardness ranged from 150.0 to 205 kg/mm², and the effective microhardness ranged from 232 to 362.3 kg/mm². The lowest value corresponds to the joint formed by the zirconium alloys and the highest value corresponds to the smoothest Ni 200 joint. The RMS percent differences for the Ni 200 tests ranged from 5.03 to 6.05%, and from 5.47 to 6.43%. The best agreement was observed with the zirconium alloys where the RMS percent difference was 3.95%.

Model and Correlation Equations for Microgap Conductance. An approximate microgap conductance model for a joint formed by conforming rough surfaces was proposed [31] that related h_g to the relative mean plane separation Y/σ and the dimensionless gas parameter M/σ

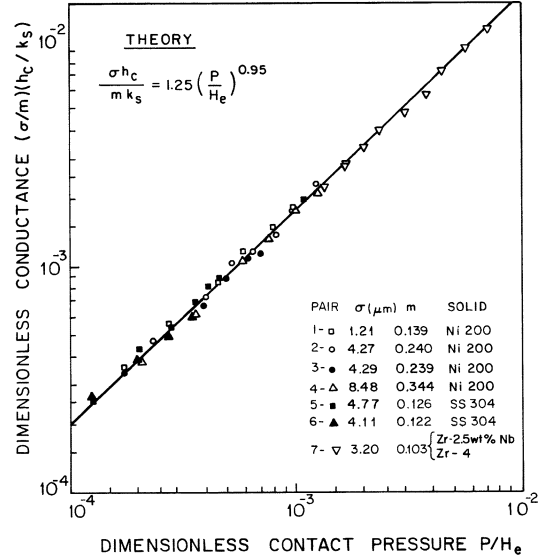


Fig. 15. Comparison of vacuum data for four metals with extended CMY model.

where $M = \alpha\beta\Lambda$. The thermal accommodation parameter is $\alpha = (2 - \alpha_1)/\alpha_1 + (2 - \alpha_2)/\alpha_2$, where α_1 and α_2 are the thermal accommodation coefficients. The gas parameter $\beta = 2\gamma/(\gamma + 1)Pr$ where $\gamma = c_p/c_v$, the ratio of the specific heats, and Pr is the Prandtl number. The molecular mean free path depends on gas pressure P_g and gas temperature T_g , $\Lambda = \Lambda_0(T_g/T_{g,0})(P_{g,0}/P_g)$. The value of the mean free path Λ_0 corresponds to $P_{g,0}$ and $T_{g,0}$.

A statistical microgap conductance model was derived in [33]. The final relation for the dimensionless microgap conductance was given in the form of an integral which was transformed into the following form which is convenient for calculations:

$$C_g = \frac{\sigma h_g}{m k_s} = \frac{\kappa}{m} \sqrt{\frac{2}{\pi}} \int_0^3 \frac{\exp\left[-\frac{(\frac{Y}{\sigma} + u)^2}{2}\right]}{u^2 + \frac{M}{\sigma}} u du = \frac{\kappa}{m} I_g \quad (43)$$

with $\kappa = k_g/k_s$ where k_g is the thermal conductivity of the gas and $k_s = 2k_1k_2/(k_1 + k_2)$. This microgap conductance model is the first one that accounts for the effect of contact pressure through the parameter Y/σ .

For quick calculations the following simple correlation equations for the gap integral was developed [62]:

$$I_g = \frac{f_g}{\frac{Y}{\sigma} + \frac{M}{\sigma}}. \quad (44)$$

In the range $2 \leq Y/\sigma \leq 4$

$$f_g = 1.063 + 0.0471 \left(4 - \frac{Y}{\sigma}\right)^{1.68} \times \left[\ln\left(\frac{\sigma}{M}\right)\right]^{0.84}, \quad \text{for } 0.01 \leq \frac{M}{\sigma} \leq 1$$

$$f_g = 1 + 0.06 \left(\frac{\sigma}{M}\right)^{0.8}, \quad \text{for } 1 \leq \frac{M}{\sigma} < \infty.$$

The correlation equations have a maximum error of approximately 2% at the two extremes $Y/\sigma = 2$ and $Y/\sigma = 4$. The microgap conductance model was validated by extensive tests with different metals, gases, and gas pressures [73], [74].

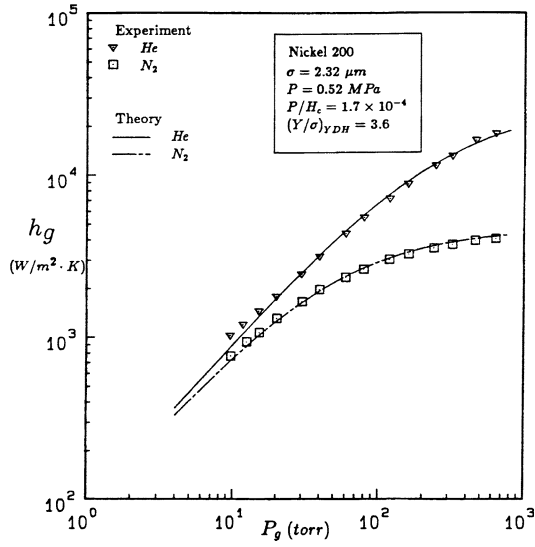


Fig. 16. Gap conductance model and data for conforming rough Ni 200 surfaces.

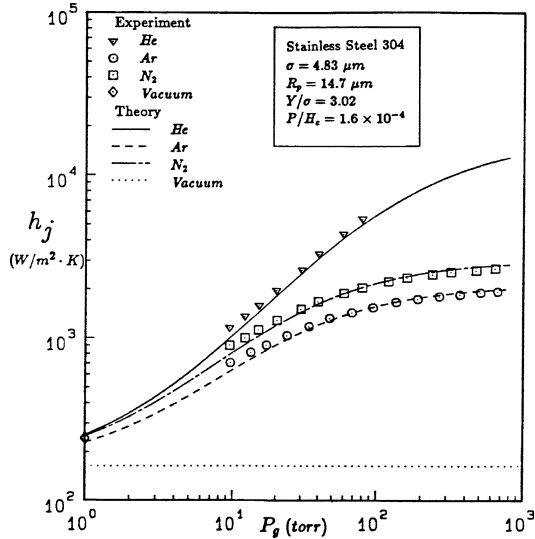


Fig. 17. Joint conductance model and data for conforming rough SS 304 surfaces.

The microgap conductance model predictions are shown as curves and the h_g data for gaseous helium and nitrogen are compared in Fig. 16 for a gap formed by a rough Ni 200 surface in contact with a lapped Ni 200 surface. The apparent contact pressure was held at 0.52 MPa while the gas pressure was varied from about 10 torr to about 700 torr. The helium gas shows values of h_g which are greater than the values for nitrogen, especially at the higher gas pressures. The agreement is excellent over the entire gas pressure range.

Fig. 17 shows the joint conductance $h_j = h_c + h_g$ data for three gases: argon, helium, and nitrogen for gas pressures in the range: $10 \leq P_g \leq 1000$ torr, and the corresponding predictions shown as three solid curves. The relative contact pressure was $P/H_c = 1.6 \times 10^{-4}$. The microgap was formed by the contact of a nominally flat rough SS 304 surface and a lapped SS 304 surface. The horizontal dotted line represents the vacuum value where $h_j = h_c$ because $h_g \ll h_c$. The agreement between

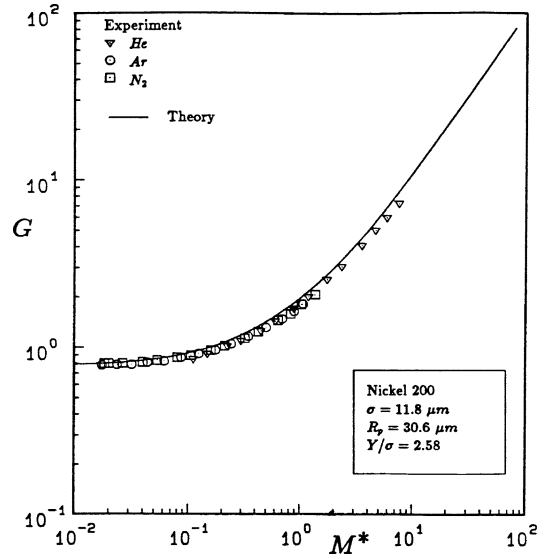


Fig. 18. Dimensionless gap conductance model and data for conforming rough Ni 200 surfaces.

the joint conductance model and the data for the three gases is excellent over the entire gas pressure range.

The dimensionless gap conductance model and data for three gases: argon, helium, and nitrogen are compared in Fig. 18 for the case where $h_c \ll h_g$ and $h_j = h_g$. The dimensionless model consists of the linear superposition of the continuum asymptote and the rarefied gas asymptote

$$G = 1 + M^* \quad (45)$$

where

$$G = \frac{k_g}{h_g Y} \quad \text{and} \quad M^* = \frac{M}{Y} = \frac{\alpha \beta \Lambda}{Y}. \quad (46)$$

The parameters are the mean plane separation Y which is related to σ and P/H_c , and the gas rarefaction parameter $M = \alpha \beta \Lambda$ which depends on the type of gas ($\gamma = c_p/c_v, Pr$), the accommodation parameter α , and the molecular mean free path Λ which depends on the gas temperature and pressure. The experimentally determined thermal accommodation coefficients for three gases were reported in [74]. The microgap was formed by the contact of a nominally flat, very rough, Ni 200 surface in contact with a lapped Ni 200 surface. All data fall on the theoretical curve. The data show the transition from the continuum asymptote where $G = 1$ to the rarefied gas asymptote where $G = M^*$.

Enhancement of Contact Conductance by Metallic Coatings. The effect of thin, soft, isotropic high thermal conductivity coatings such as a silver layer on a Ni 200 substrate was studied analytically and experimentally [38], [44]. A mechanical model was developed for the prediction of effective microhardness of a hard conforming rough surface placed in contact with a smooth silver layer bonded to a Ni 200 substrate. A thermal contact conductance model was also developed which is based on the results from the mechanical model.

The Vickers microhardness measurements of the effective microhardness versus the relative layer thickness t/d are shown in Fig. 19. The layer thickness is t and the depth of indentation is d .

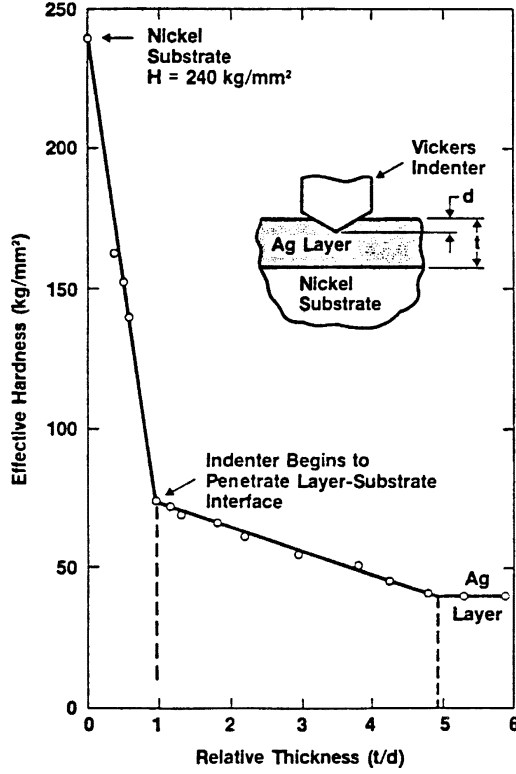


Fig. 19. Vickers microhardness of silver layer on nickel substrate.

The measured values of microhardness were obtained using several layer thicknesses and several loads. There are three regions based on the values of t/d . For thin layers where $0 < t/d \leq 1$, the effective microhardness is large but less than the microhardness of the substrate H_S because some of the load is supported by the layer as the indenter penetrates the substrate. The second region corresponds to the interval $1 \leq t/d \leq 4.9$, where more of the load is supported by the layer and less by the substrate. For the third region where $t/d \geq 4.9$, the indenter penetrates the layer only and the presence of the substrate can be neglected, and the effective microhardness is equal to the hardness of the layer H_L .

The effective Vickers microhardness measurements are denoted as H' . The three microhardness regions were correlated as

$$H' = H_S \left(1 - \frac{t}{d}\right) + 1.81H_L \left(\frac{t}{d}\right), \quad \text{for } 0 \leq \frac{t}{d} < 1.0 \quad (47)$$

$$H' = 1.81H_L - 0.21H_L \left(\frac{t}{d} - 1\right), \quad \text{for } 1.0 \leq \frac{t}{d} \leq 4.90 \quad (48)$$

$$H' = H_L, \quad \text{for } \frac{t}{d} > 4.90 \quad (49)$$

where H_S and H_L are the substrate and layer microhardness respectively. The Ni 200 substrate microhardness is $H_S = 2.97$ GPa for the joint roughness parameter values:

$\sigma = 4.27 \mu\text{m}$ and $m = 0.236$ rad. The Vickers microhardness of the silver layer is $H_L = 40 \text{ kg/mm}^2 = 0.394$ GPa.

The relative indentation depth is obtained from the following approximate correlation equation [38], [44]:

$$\frac{t}{d} = 1.04 \left(\frac{t}{\sigma}\right) \left(\frac{P}{H'}\right)^{-0.097} \quad (50)$$

To implement the procedure for finding H' from the three correlation equations requires an iterative method. To initiate the iterative process, the first guess may be based on the arithmetic average of the substrate and layer microhardness values

$$H'_1 = \frac{H_S + H_L}{2}.$$

For a given value of t and P , the first value of t/d can be computed. From the three correlation equations one can find a new value for H' , say H'_2 . The new microhardness value, H'_2 , is used to find another value for t/d which leads to another value H'_3 . The process is continued until convergence according to some criterion occurs. This usually happens within three to four iterations.

Once the effective microhardness is known, then the microcontact spot radius a , and the number of microcontacts N , can be calculated for the given values of the parameters: (P, A_a, σ, m) . The overall thermal resistance of a joint formed by a nominally flat rough surface of thermal conductivity k_1 and a smooth, silver layer of thermal conductivity k_3 and uniform thickness t which bonded to a smooth Ni 200 substrate of thermal conductivity k_2 is

$$R_j = \frac{R_{c,i}}{N} \quad (51)$$

where the total number of microcontact spots N depends on the apparent area A_a , the apparent contact pressure P , the effective microhardness of the joint H' , and the mean contact spot radius a . From a force balance we have

$$N = \frac{PA_a}{H'\pi a^2}. \quad (52)$$

The total constriction-spreading resistance of the i th microcontact spot is

$$R_{c,i} = \frac{\psi}{2a} \left(\frac{k_2 + Ck_1}{2k_1k_2}\right) = \frac{\psi}{2ak'} \quad (53)$$

where k' is the effective thermal of the joint. It consists of the thermal conductivities k_1 and k_2 , and the parameter C which accounts for spreading in the silver layer and the substrate. This parameter is defined as

$$C = \frac{\psi_{23}}{\psi_2} \quad (54)$$

where ψ_{23} is the spreading resistance parameter in the silver layer and substrate, and ψ_2 is the spreading resistance in the substrate when the layer is absent. Its given by the relation

$$\psi_{23} = \frac{8}{\pi\epsilon} \sum_{n=1}^{\infty} \frac{J_1(\delta_n\epsilon) \sin \delta_n\epsilon}{\delta_n^3 J_0^2(\delta_n)} \varphi_n \quad (55)$$

where $J_0(\delta_n)$ and $J_1(\delta_n)$ are Bessel functions of the first kind of order 0 and 1, and δ_n are the positive roots of $J_1(\delta_n) = 0$.

The layer-substrate parameter φ_n depends on relative contact spot size $\epsilon = a/b$, relative layer thickness $\tau = t/a$, and substrate-to-layer thermal conductivity ratio $\kappa = k_2/k_3$. Its given by the relation

$$\varphi_n = \kappa \left[\frac{(1 + \kappa) + (1 - \kappa) \exp(-2\delta_n \epsilon \tau)}{(1 + \kappa) - (1 - \kappa) \exp(-2\delta_n \epsilon \tau)} \right]. \quad (56)$$

If $\kappa = 1$, the thermal conductivities of the layer and substrate are identical, and $\varphi_n = 1$, $n = 1, 2, 3, \dots$. If the layer thickness is much greater than the contact spot radius, i.e., $\tau \gg 1$, then $\varphi_n = \kappa$, and the spreading resistance becomes $\psi_3/4ak_3$.

The total constriction-spreading resistance of the single circular microcontact spot has two limits which depend on the relative layer thickness

$$R_{c,i} = \begin{cases} \frac{\psi_1}{4ak_1} + \frac{\psi_2}{4ak_2} & \frac{t}{a} \rightarrow 0 \\ \frac{\psi_1}{4ak_1} + \frac{\psi_3}{4ak_3} & \frac{t}{a} \rightarrow \infty. \end{cases} \quad (57)$$

Because of geometric symmetry about the contact plane we have $\psi_1 = \psi_2 = \psi_3 = \psi = (1 - \epsilon)^{3/2}$ for $\epsilon < 0.3$. The relative contact spot size is $\epsilon = (P/H')^{1/2}$.

The joint conductance and contact conductance are equal for a vacuum when radiation heat transfer is negligible, i.e., $h_j = h_c$. The contact conductance is given by

$$h_c = \frac{1}{A_a R_j}. \quad (58)$$

It was shown [38], [44] that the dimensionless contact conductance is given by

$$C_c = \left(\frac{\sigma}{m} \right) \left(\frac{h_c}{k'} \right) = 1.25 \left(\frac{P}{H'} \right)^{0.95} \quad (59)$$

where the effective joint thermal conductivity k' replaces k_s and the effective microhardness H' replaces the contact microhardness H_c in the extended CMY model for conforming rough surfaces. For details of the application of the mechanical and thermal models to some problems from the microelectronics industry, the reader should consult [38], [44].

The vacuum data for four different joints were compared with the extended CMY model. The dimensionless contact conductance $C_c = (\sigma/m)(h_c/k_s)$ versus the relative contact pressure P/H_c are compared with the CMY model correlation equation in Fig. 20. The nominal surface roughness levels were $\sigma = 1.28, 4.27, 8.32 \mu\text{m}$, and the nominal values of the corresponding mean absolute asperity slopes were $m = 0.14, 0.24, 0.34$ rad. The bulk hardness of the Ni 200 substrate was $H_B = 1.70$ GPa, and the calculated microhardness, based on the average contact pressure $P = 2$ MPa were $H_c = 3.60, 3.00, 2.80$ GPa, respectively. The less rough surface had the highest contact microhardness, while the roughest surface had the smallest contact microhardness. The agreement between the model prediction and all bare surface data is very good.

Fig. 21 shows plots for two similar joints with $\sigma = 4.27 \mu\text{m}$ and $m = 0.24$ rad. The vacuum data of the contact conductance

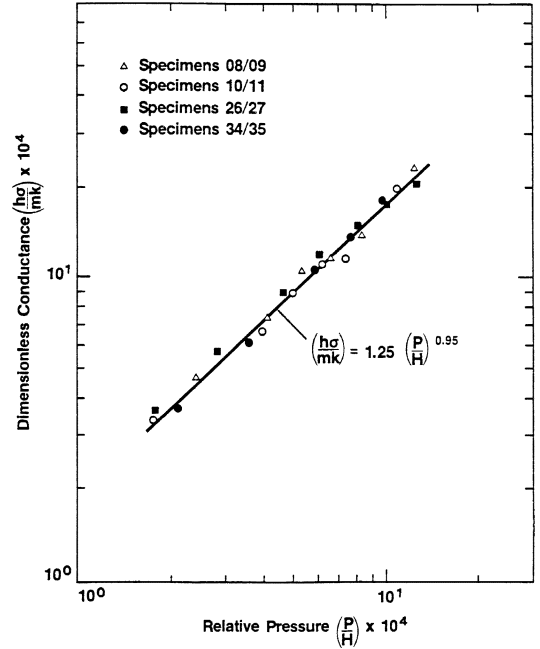


Fig. 20. Comparison of Ni 200 vacuum data and extended CMY model.

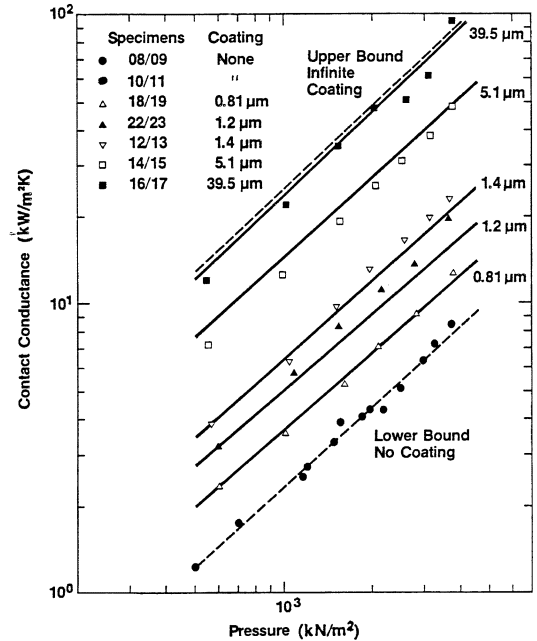


Fig. 21. Contact conductance data and model predictions versus contact pressure.

of the bare surface denoted as the lower bound corresponding to no coating, and the data corresponding to different layer thicknesses. The layer thickness was varied from a very thin layer of thickness $0.81 \mu\text{m}$ to a very thick layer of thickness $39.5 \mu\text{m}$.

The data for the very thick layer were close to values corresponding to the upper bound for $t/d \geq 4.9$, called the "infinitely" thick coating. It is seen that a thin layer of silver significantly increases the contact conductance. There is approximately a tenfold increase in the values of h_c for $t > 5 \mu\text{m}$.

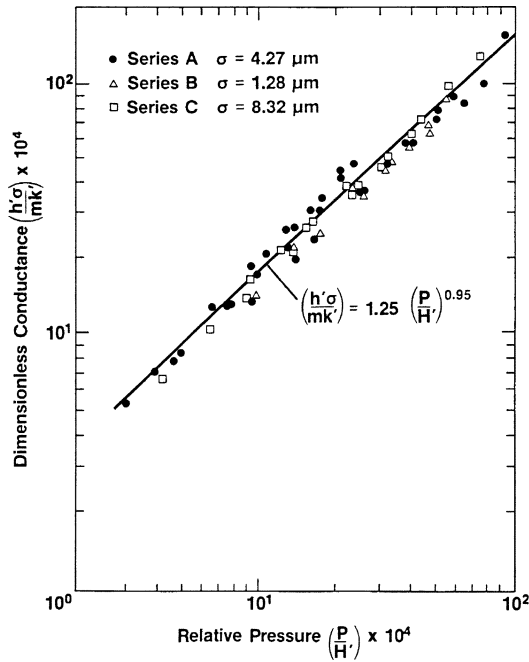


Fig. 22. Dimensionless contact conductance versus dimensionless contact pressure: all data and CMY model.

For all tests the model predictions and the data exhibit similar trends with contact pressure, they are in very good agreement for all contact pressures and layer thicknesses. The RMS difference for all bare surface data and the extended CMY model is 9.3%.

All of the bare surface data and the data with silver layers of different thicknesses for the three joints are shown in Fig. 22. The dimensionless contact conductance is denoted as $C_c = (h'/k')(\sigma/m)$ where the primes denote the enhanced values of contact conductance and the effective thermal conductivity of the joint. The relative contact pressure is P/H' where H' is the effective contact microhardness which varies from $H' = H_S$ when $t = 0 \mu\text{m}$ to $H' = H_L$ when $t > 5 \mu\text{m}$.

All data fall on or lie near the theoretical curve $C_c = 1.25 (P/H')^{0.95}$ which is the extended CMY model. The RMS difference between all coated joints and the correlation equation of the extended CMY model is 11.8%.

The extended CMY model was used to calculate the enhancement of contact conductance due to layer thickness for Lead, Tin, silver and Copper for a rough Ni 200 surface in contact with a lapped Ni 200 surface at a contact pressure of $P = 2000 \text{ kPa}$, and surface roughness of $\sigma = 4.27 \mu\text{m}$ and absolute mean asperity slope of $m = 0.234 \text{ rad}$. The nominal values of the thermal conductivity and the microhardness of the coatings are listed in Table VII.

The calculated values are shown in Fig. 23. The curves for each metal reveal three regions corresponding to the three regions of the Vickers microhardness measurements. As the layer thickness increases there is a significant increase (enhancement) in the contact conductance for all metals. The best metal is Lead, followed by Tin because the enhancement is more than a factor of 10. The metal that shows the smallest increase is Copper because its harder than the other metals.

TABLE VII
ASSUMED NOMINAL PROPERTY VALUES OF FOUR COATINGS

	$k(\text{W/m} \cdot \text{K})$	$H(\text{kg/mm}^2)$
Lead	32.4	3.0
Tin	58.4	8.5
Silver	406	40
Copper	376	85

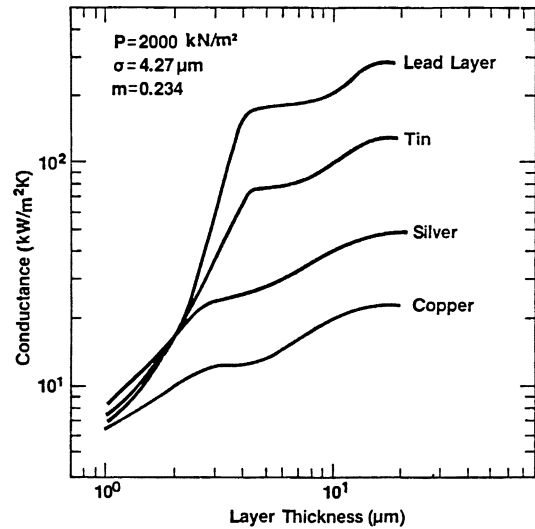


Fig. 23. Contact conductance versus layer thickness for lead, tin, silver, and copper.

VII. THERMAL CONTACT RESISTANCE RESEARCH 1990–2004

During the period 1990–2004 the research on TCR dealt with constriction-spreading resistances of single and multiple heat sources; transient spreading resistance; micro and macrogap resistances and conductances; elastic, plastic and elastoplastic contact models for conforming rough surfaces of several metals; experiments to determine the effects of surface conditions on thermal accommodation coefficients for helium, nitrogen, and argon; mechanical contact and constriction resistance models and experiments for smooth hemisphere-smooth layer bonded to substrate joints; models and experiments for bolted joints for microelectronics and satellite applications; and related miscellaneous studies such as the effect of surface asperity truncation at light loads, and the role of spreading resistance on the effective thermal conductivity of laminated substrates [94], and related topics [93], [95].

Constriction-Spreading Resistances. The results of the analytical and numerical work on thermal constriction-spreading resistance in different systems appeared in several papers [80], [89], [91], [97], [106]. Most of the important results are summarized in Chapter 4 [105]. The effect of multiple layers [86] and transient effects [87] on constriction-spreading have been examined. The thermal interaction of multiple sources on rectangular systems are presented in [107].

Micro and Macrogap Resistance and Conductance. Additional research was done to complement and extend the earlier models for thermal resistances and conductances for microgaps [74], [75], [111] and macrogaps [112]. The microgap model was compared with extensive tests conducted with different surface

roughness levels, Ni 200 and SS 304 surfaces, and the test gases were helium and nitrogen [74], [75]. Compact gap resistance models for microgaps [111] and macrogaps [112] were developed. The agreement between the data and the models was very good.

Bolted Joints. The results of the analytical and experimental research on bolted joints for applications to microelectronics [76] and to satellites [79], [85], [88], [90] was done in this period. Some of the results for satellites applications appear in [104]. Since bolted joints are complex geometric systems, the mechanical models are unique to the particular system. The associated thermal models are also unique. Its beyond the scope of this review article to present the important results.

Effect of Single Layer on Sphere-Flat Contact. The earlier analytical and experimental research on the effect of a single layer bonded to a substrate on the joint resistance of the sphere-flat contact was re-examined and extended to include softer, low conductivity, polymeric layers [92], [96]. The important results are summarized in [105].

Elastoplastic Contact Model for Sphere-Flat Joint. The elastoplastic contact model for the smooth sphere-smooth flat joint was presented in [81]. Under vacuum conditions and negligible radiative heat transfer across the macrogap, the total joint resistance is given by

$$R_c = \frac{(1 - \frac{a}{b})^{1.5}}{2ak_s} \quad (60)$$

where a is the contact radius, b is the radius of the flat and the rod with the hemispherical end whose radius of curvature is β . The effective thermal conductivity of the hemisphere and flat is $k_s = 2k_1k_2/(k_1 + k_2)$.

The relative elastoplastic contact radius is given by [81]

$$\left(\frac{a}{\beta}\right)_{ep} = \left[\left(\frac{a}{\beta}\right)_e^n + \left(\frac{a}{\beta}\right)_p^n \right]^{\frac{1}{n}}. \quad (61)$$

The subscripts e , p and ep denote pure elastic, pure plastic, and elastoplastic deformation. The value of the ‘‘fitting’’ parameter n can be found from a comparison of the model with experimental data. It was found to be close to $n = 5$. The elastic contact occurs when the contact force F is smaller than the critical force F_c , say, $F \leq 0.05F_c$, and the plastic contact occurs when $F \geq 20F_c$. The critical force is obtained by equating the elastic contact radius a_e and the plastic contact radius a_p . Therefore

$$F_c = 366.7 \left(\frac{S_f}{E'}\right)^2 \beta^2 S_f. \quad (62)$$

The critical force is a complex parameter that depends on the elastic and plastic properties, and the radius of curvature. The presence of the flow stress makes the relation complex.

For pure elastic contact the relative contact radius is [81]

$$\left(\frac{a}{\beta}\right)_e = \left(\frac{3F\beta}{4E'}\right)^{\frac{1}{3}} \quad (63)$$

where the equivalent elastic modulus is

$$E' = \left(\frac{1 - \nu_1^2}{E_1} + \frac{1 - \nu_2^2}{E_2}\right)^{-1}. \quad (64)$$

The elastic properties of the contacting hemisphere and flat are, respectively, E_1, ν_1, E_2, ν_2 .

For pure plastic contact the relative contact radius is [81]

$$\left(\frac{a}{\beta}\right)_p = \left(\frac{F}{\pi C_p S_f}\right)^{\frac{1}{2}} \quad (65)$$

where $C_p = H/S_f = 2.76$ is the plastic constraint parameter, and the normal indentation hardness is $H = F/\pi a_p^2$. The ratio of hardness H to the flow stress S_f under fully plastic deformation is a constant for real strain hardening materials provided the appropriate value of S_f is used. There are currently no mechanical models to predict the flow stress; therefore, it must be obtained from experiments for each metal. If, however, the deformation is fully plastic, then

$$S_f = \frac{H_B}{C_p} \quad (66)$$

where H_B is the Brinell hardness (bulk hardness). An iterative procedure was presented in [81] for calculating the value of S_f for a particular contact based on the measured contact resistance.

The validity and accuracy of the elastoplastic contact model were established by comparisons of the predictions and vacuum test results [81]. Fig. 24 shows the very good agreement of the dimensionless contact resistance $R_c^* = 2bk_s R_c$ plotted against the relative contact radius b/a . The vacuum data are from two research programs, and they clearly exhibit pure elastic deformation and elastoplastic deformation of the flat because the hemispheres are harder.

Empirical Methods for Prediction of Vickers Microhardness. The experimental research on thermal contact conductance was continued to include tool steels which have hardened surfaces due to heat treatments [82]. The Vickers, Brinell and Rockwell microhardness and hardness measurements were made on tool steels at room temperature and at elevated temperatures (200 °C). The untreated Brinell hardness was about 2 GPa, and the heat treated Brinell hardness ranged from 2.2 to 7.6 GPa. The Vickers microhardness correlation coefficients c_1 and c_2 first reported, correlated, and used in [32], [35], [63] were extended to a much wider range of Brinell hardness: 1.3–7.6 GPa. The least-squares cubic fits gave the following correlation equations [83]:

$$c_1 = 3178 \left[4.0 - 5.77H_B^* + 4.0(H_B^*)^2 - 0.61(H_B^*)^3 \right] \quad (67)$$

and

$$c_2 = -0.57 + \frac{1}{1.22}H_B^* - \frac{1}{2.42}(H_B^*)^2 + \frac{1}{16.58}(H_B^*)^3 \quad (68)$$

where the dimensionless Brinell hardness is defined as $H_B^* = H_B/3178$, and the units of H_B are MPa. An alternative correlation was presented for c_2 in terms of H_B and c_1

$$c_2 = -0.370 + 0.442 \left(\frac{H_B}{c_1}\right). \quad (69)$$

The extended correlation equations for c_1 and c_2 give acceptable accuracy when compared with the correlation equations developed specifically for Ni 200, SS 304, and the zirconium

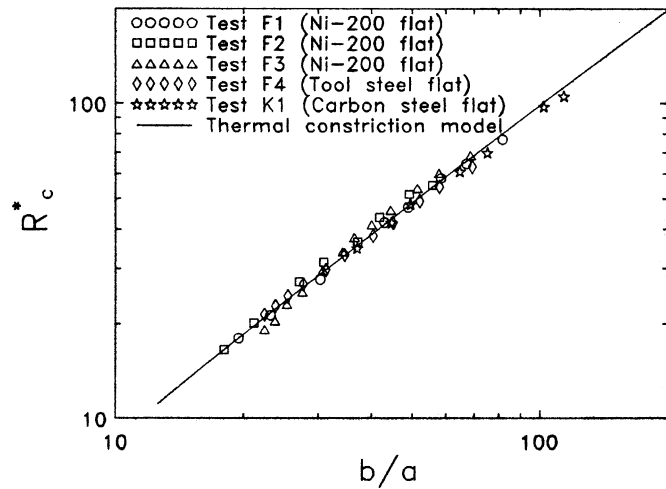


Fig. 24. Elastoplastic contact resistance model and vacuum data of hemisphere-flat joints.

alloys. The correlation equations can be used to predict the contact microhardness H_c of conforming rough surfaces given the parameters: (H_B, σ, m) , and the apparent contact pressure P .

Elastoplastic Contact Conductance Model for Conforming Rough Surfaces. The elastic contact models [Greenwood and Williamson (GW), Bush, Gibson and Thomas (BGT), Whitehouse and Archard (WA), Mikic, and Majumdar and Tien (MT)] for conforming rough surfaces were reviewed and compared [78]. The elastic contact models are complex because they are based on surface roughness parameters that cannot be measured by conventional surface profilometers. The elastic contact model of Mikic [78] is the “simplest” model because it requires only σ and m which are easily measured, and they have been reported for several metals which have undergone extensive thermal contact conductance tests.

It was shown that GW, and the WA elastic contact conductance models are comparable when they were compared with the elastic contact conductance model of Mikic. The Mikic model predictions lie close to the lowest values predicted by the GW and WA models. The predictions of the BGT model fall well below the predictions of the Mikic model.

The elastic contact model of Majumdar and Tien is based on a fractal network. This model is very different from the other elastic contact models, and, therefore, could not be compared.

In the review of the several elastic contact models for conforming rough surfaces [78] and comparisons with vacuum data for Ni 200, SS 304, and the zirconium alloys (Zr-4, Zr-Nb), it was observed that there are major differences between the respective models, and that there is poor agreement with the data.

In Fig. 25, the Ni 200 vacuum data for several joints are compared with the elastic contact model of Mikic and extended plastic contact model [78]. In the elastic and plastic contact models the dimensionless contact conductance $(\sigma/m)(h_c/k_s)$ are identical; however, the dimensionless contact pressures are different. For the elastic model of Mikic [78] the relative contact pressure is $\sqrt{2}P/mE'$ and for the plastic model its P/H_c .

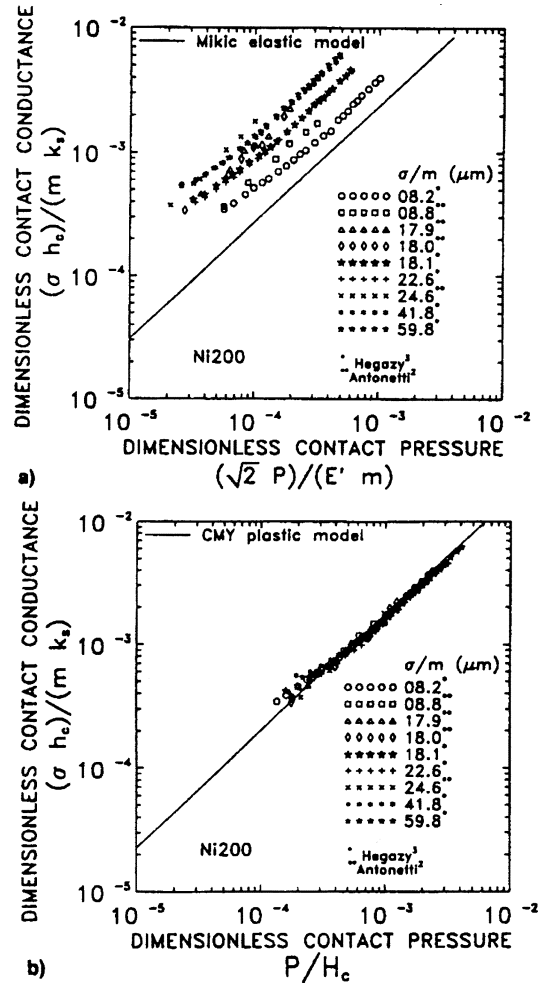


Fig. 25. Ni 200 data versus elastic and plastic contact conductance models.

All Ni 200 data lie well above the elastic curve and they are “scattered.” All Ni 200 data are “clustered” together and lie on the plastic curve. In Fig. 26, the SS 304 vacuum data for several joints are compared with the elastic and plastic models. The trends observed with the Ni 200 data are similar except for three joints which show very good agreement with the elastic model. There is good to very good agreement between all SS 304 data and the plastic model. There is, however, slightly more “scatter” than observed with the Ni 200 data. Its interesting to note that the data of three joints are equally well predicted by the elastic and plastic contact models. The SS 304 data of McWaid showed considerable scatter when compared with the elastic and plastic contact conductance models.

An elastoplastic contact model for conforming rough surfaces was developed [84] based on the concepts developed for the sphere-flat contact [81]. Since the full development is beyond the scope of this review article, only the results and relations of the elastoplastic contact model will be presented and compared with the Ni 200 and SS 304 vacuum data. The elastoplastic contact model is based on the elastic model and the plastic model as described in [78], [81]. To have a common basis the elastoplastic microhardness H_{ep} was introduced.

The results are summarized below in terms of the geometric parameters: i) A_r/A_a , the real to apparent area ratio, ii) n , the

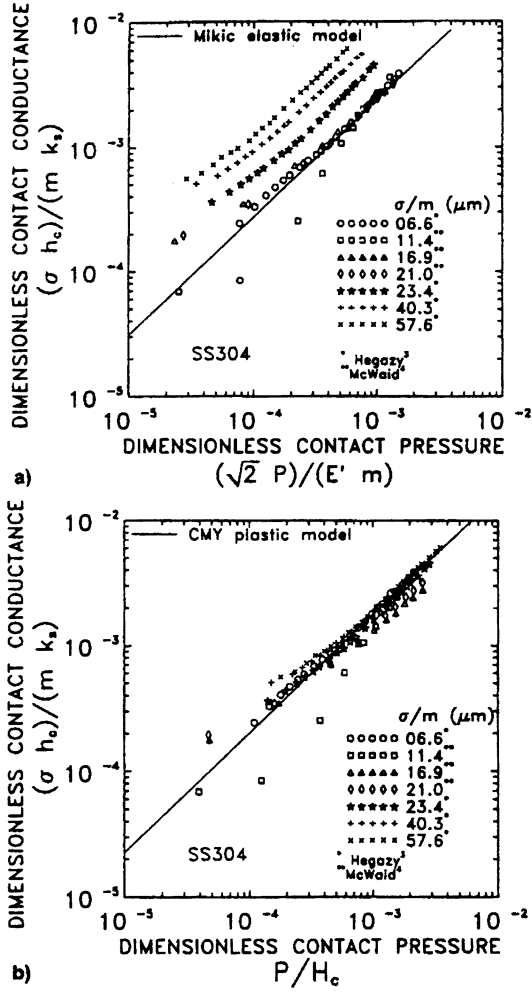


Fig. 26. SS 304 data versus elastic and plastic contact conductance models.

contact spot density, iii) a , the mean contact spot radius, and iv) λ , the relative mean plane separation [84]

$$\left. \begin{aligned} \frac{A_r}{A_a} &= \frac{f_{ep}}{2} \operatorname{erfc}\left(\frac{\lambda}{\sqrt{2}}\right) \\ n &= \frac{1}{16} \left(\frac{m}{\sigma}\right)^2 \frac{\exp(-\lambda^2)}{\operatorname{erfc}\left(\frac{\lambda}{\sqrt{2}}\right)} \\ a &= \sqrt{\frac{8}{\pi}} \sqrt{f_{ep}} \left(\frac{\sigma}{m}\right) \exp\left(\frac{\lambda^2}{2}\right) \operatorname{erfc}\left(\frac{\lambda}{\sqrt{2}}\right) \\ na &= \frac{1}{8} \sqrt{\frac{2}{\pi}} \sqrt{f_{ep}} \left(\frac{m}{\sigma}\right) \exp\left(-\frac{\lambda^2}{2}\right) \\ \frac{\sigma h_c}{m k_s} &= \frac{1}{2\sqrt{2}\pi} \frac{\sqrt{f_{ep}} \exp\left(-\frac{\lambda^2}{2}\right)}{\left[1 - \sqrt{\frac{f_{ep}}{2}} \operatorname{erfc}\left(\frac{\lambda}{\sqrt{2}}\right)\right]^{1.5}} \\ \lambda &= \sqrt{2} \operatorname{erfc}^{-1}\left(\frac{1}{f_{ep}} \frac{2P}{H_{ep}}\right) \end{aligned} \right\} \quad (70)$$

The elastoplastic parameter f_{ep} is a function of the dimensionless contact strain ϵ_c^* which depends on the amount of work hardening. This physical parameter lies in the range:

$0.5 \leq f_{ep} \leq 1.0$. The smallest and largest values correspond to zero and infinitely large contact strain respectively. The elastoplastic parameter is related to the contact strain [84]

$$f_{ep} = \frac{\left[1 + \left(\frac{6.5}{\epsilon_c^*}\right)^2\right]^{1/2}}{\left[1 + \left(\frac{13.0}{\epsilon_c^*}\right)^{1.2}\right]^{1/2}}, \quad 0 < \epsilon_c^* < \infty. \quad (71)$$

The dimensionless contact strain is defined as [84]

$$\epsilon_c^* = 1.67 \left(\frac{mE'}{S_f}\right) \quad (72)$$

where S_f is the material yield or flow stress, a complex physical parameter, which must be obtained by contact experiments for each metal.

The elastoplastic microhardness H_{ep} can be determined by means of an iterative procedure which requires the following relationship [84]:

$$H_{ep} = \frac{2.76S_f}{\left[1 + \left(\frac{6.5}{\epsilon_c^*}\right)^2\right]^{1/2}}. \quad (73)$$

The proposed elastoplastic contact conductance model “moves” smoothly between the elastic and plastic contact conductance models. The dimensionless contact pressure for elastoplastic deformation of the contacting asperities is obtained from the following approximate explicit relation [84]

$$\frac{P}{H_{ep}} = \left[\frac{0.9272P}{c_1 \left(\frac{1.43\sigma}{m}\right)^{c_2}} \right]^{\frac{1}{1+0.071c_2}} \quad (74)$$

where the coefficients c_1 , c_2 are obtained from Vickers microhardness tests.

The complex elastoplastic contact model is approximated by the following correlation equations for the dimensionless contact conductance [84]

$$C_c = \begin{cases} 1.54 \left(\frac{P}{H_{ep}}\right)^{0.94}, & 0 < \epsilon_c^* < 5 \\ 1.245b_1 \left(\frac{P}{H_{ep}}\right)^{b_2}, & 5 < \epsilon_c^* < 400 \\ 1.25 \left(\frac{P}{H_{ep}}\right)^{0.95}, & 400 < \epsilon_c^* < \infty \end{cases} \quad (75)$$

The elastoplastic correlation coefficients (b_1, b_2) depend on the dimensionless contact strain [84]

$$b_1 = \left(1 + \frac{46690.2}{(\epsilon_c^*)^{2.49}}\right)^{\frac{1}{30}} \quad (76)$$

and

$$b_2 = \left[\frac{1}{1 + \frac{2086.9}{(\epsilon_c^*)^{1.842}}}\right]^{\frac{1}{600}} \quad (77)$$

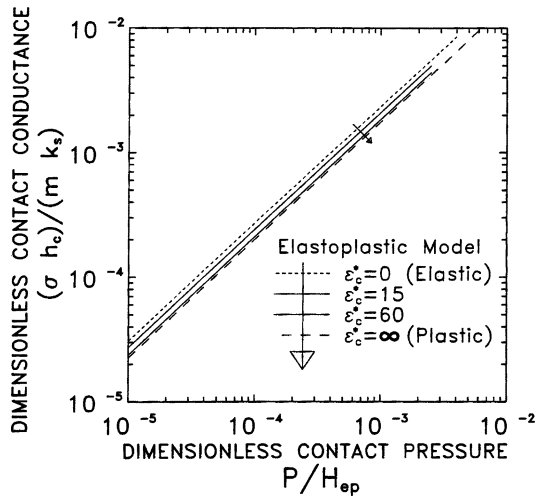


Fig. 27. Elastoplastic contact conductance model versus relative contact pressure.

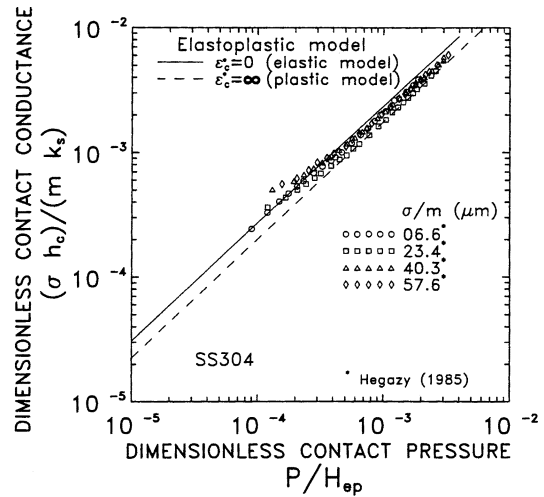


Fig. 29. SS 304 data versus elastoplastic contact conductance model.

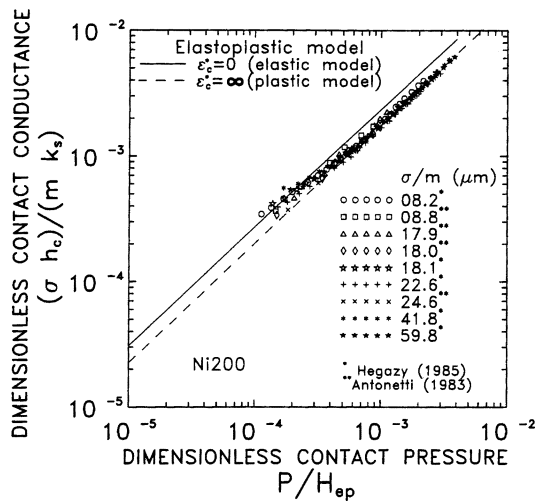


Fig. 28. Ni 200 data versus elastoplastic contact conductance model.

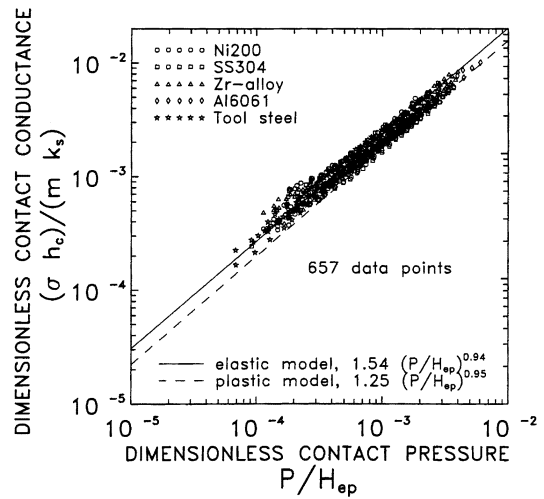


Fig. 30. All vacuum data versus elastoplastic contact conductance model.

The elastoplastic contact conductance model is shown as dimensionless contact conductance $C_c = (\sigma/m)(h_c/k_s)$ plotted versus the relative contact pressure P/H_{ep} for four values of the dimensionless contact strain ϵ_c^* in Fig. 27. The elastic contact curve $\epsilon_c^* = 0$ and plastic contact curve $\epsilon_c^* = \infty$ represent upper and lower bounds on the dimensionless contact conductance. The elastic curve lies above and is essential parallel to the plastic curve for the wide range of relative contact pressure: $10^{-5} \leq P/H_{ep} \leq 10^{-2}$.

The elastoplastic contact conductance model was validated by comparisons with vacuum data for five metals. Figs. 28–30 show the dimensionless contact conductance $(\sigma/m)(h_c/k_s)$ plotted against the relative contact pressure P/H_{ep} .

Fig. 28 shows comparisons between the Ni 200 vacuum data and the elastoplastic contact conductance model. The Ni 200 data generally lie on or near the plastic curve at the high contact pressures and they lie between the curves and tend to move closer to the elastic curve at the lowest contact pressures. The data are essentially together.

Fig. 29 shows comparisons between the SS 304 vacuum data and the elastoplastic contact conductance model. The SS 304

data show similar trends to the Ni 200 data, however, here more of the data lie between the two curves. At the lowest contact pressures some of the points lie on the elastic curve, and some fall above the elastic curve.

Fig. 30 shows 657 vacuum data points for Ni 200, SS 304, the zirconium alloys (Zr-4, Zr-Nb), Al 6061, and the heat treated tool steel [82] compared with the elastoplastic model. Most of the data fall between the two bounds. The hard heat treated tool steel data lie closer to the elastic curve. Some data corresponding to the lowest contact pressures fall above the elastic curve. This trend is thought to be due to the asperity truncation effect [102], [103] which has been observed with very rough surfaces at the lowest contact pressures.

Thermal Interface Materials (TIMs). The issues associated with the effects of thermal interface materials (TIMs) on thermal joint conductance or resistance were examined and reported in four publications [98]–[101]. A comprehensive review [98] examined the various types of TIMs that can be used to “enhance” joint conductance, and the available thermomechanical models. From this review, its concluded that its not possible to develop a single comprehensive model that can predict accurately the

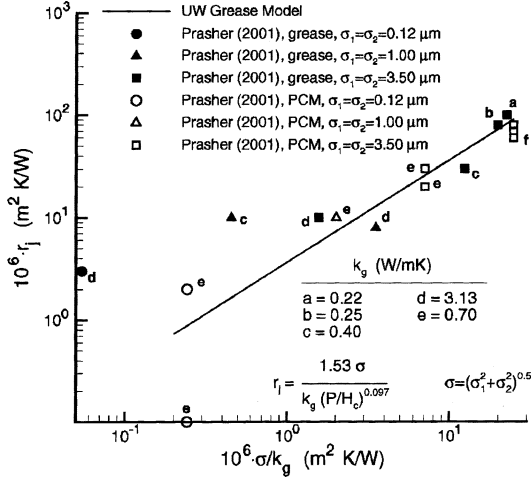


Fig. 31. Comparison of grease and phase change data with simple joint model.

joint conductance of the difference TIMs and joints. The definitions of thermal contact conductance and resistance, the effective thermophysical properties, and various published models were examined in [100], and experiments and data were presented in [101].

A simple joint resistance and conductance model for grease filled joints, and relations were presented in [99]. The model was developed for conforming rough surfaces under light contact pressures. The surface roughness is assumed to be gaussian, and the relations for plastic contact were used. The effective thickness of the microgaps is characterized by the mean plane separation Y . The microgaps are assumed to be occupied with a substance (e.g., oil, grease, grease filled with solid particles) that is isotropic and homogeneous, and that it perfectly wets the bounding surfaces. The substance is opaque to radiation heat transfer. The thermal conductivity of the substance k_g is assumed to be constant.

The simple model for a substance in the microgaps is based on the assumption that $h_g \gg h_c$, and, therefore, $h_j = h_g$, and the specific joint resistance is $r_j = 1/h_j$. The joint conductance is modeled as

$$h_j = \frac{k_g}{Y} = \frac{k_g \sigma}{Y}. \quad (78)$$

The relative mean plane separation is given by the approximation

$$\frac{Y}{\sigma} = 1.53 \left(\frac{P}{H_c} \right)^{-0.097}. \quad (79)$$

The microhardness is given by the following approximation:

$$H_c = (12.2 - 3.54H_B) \left(\frac{10^6 \sigma}{m} \right)^{-0.26} \quad (80)$$

where the units of H_c and H_B are GPa, and the units of σ/m are μm . The simple model is compared with grease filled with solid particles and phase change materials in Fig. 31. The bounding surfaces of the joint are pure copper with a microhardness of $H_c = 0.8$ GPa. The surface roughness values and the effective thermal conductivities of the grease and phase change materials

are given in the legend of the figure. The specific joint resistance $10^6 r_j$ is plotted against the parameter $10^6 \sigma/k_g$ for $P = 0.1$ MPa (see Fig. 31).

The trends of the data and the model are similar, and the agreement between the data and model is good except for the smallest values of $10^6 \sigma/k_g$. This corresponds to the smallest microgap thickness and the largest effective thermal conductivity. The discrepancies may be attributed to the fact that the mean particle size is comparable or larger than the mean thickness of the microgap.

Compact Models for Conforming and Nonconforming Rough Surfaces. Extensive research [108]–[114] was done to develop compact models for thermal joint resistance that can handle in a seamless manner the mechanical contact of conforming and nonconforming surfaces, and heat transfer across the formed joints in a vacuum or with a gas occupying the micro and macrogaps. The compact model is complex because it accounts for the mechanical interaction of the micro (surface roughness) and macro (curvature) geometry of a joint. Elastic, plastic and elastoplastic contact models were developed, and the predictions were compared with available data [108], [110], [114], and good agreement was observed.

The scale analysis [109] for contacts in a vacuum yielded the following relation for the dimensionless joint resistance:

$$R_j^* = 2k_s L R_j = \frac{0.36}{P^*} + \frac{L \left(1 - \frac{a_L}{b_L}\right)^{1.5}}{a_L} \quad (81)$$

where the first term on the right hand side represents the micro-resistance and the second term represents the macro-resistance. The dimensionless geometric parameter is $L = b_L/(\sigma/m)$ and the dimensionless contact pressure is $P^* = F/(\pi b_L^2 H^*)$. The dimensionless microhardness is related to the Vickers microhardness correlation coefficients (c_1, c_2), and the effective surface roughness: $H^* = c_1(\sigma/m\sigma_0)^{c_2}$ where $\sigma_0 = 1 \mu\text{m}$ is the reference roughness value. The macrocontact radius

$$a_L = 1.80 a_H \frac{\sqrt{\alpha + 0.31\tau^{0.056}}}{\tau^{0.028}} \quad (82)$$

is related to the Hertz contact radius for smooth surfaces

$$a_H = \left(\frac{3F\rho}{4E'} \right)^{\frac{1}{3}} \quad (83)$$

where F is the total axial force on the joint, ρ is the radius of curvature, and E' is the effective modulus of elasticity. The dimensionless micro and macrogeometric parameters are related to the Hertz contact radius

$$\alpha = \frac{\sigma\rho}{a_H^2} \quad \text{and} \quad \tau = \frac{\rho}{a_H}. \quad (84)$$

The dimensionless macro-to-micro resistance ratio parameter was introduced

$$\Theta = \frac{R_L}{R_s} = \frac{F \left(1 - \frac{a_L}{b_L}\right)^{1.5}}{1.13 \left(\frac{\sigma}{m}\right) a_L H^*}. \quad (85)$$

This important parameter includes the applied force F , the micro and macro-geometrical parameters: (σ, m, ρ, b_L), as well as the physical properties of the contacting bodies E' and H^* . This parameter shows that the compact model goes

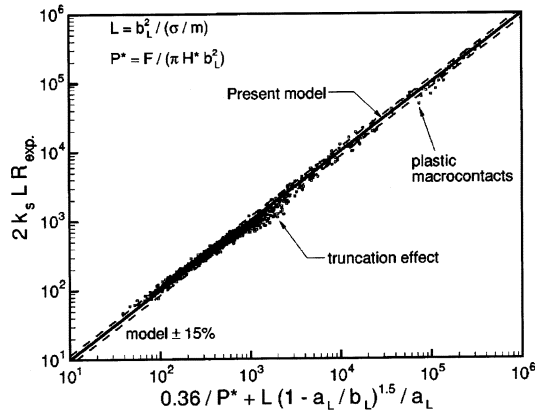


Fig. 32. Comparison of compact model with conforming rough surface vacuum data.

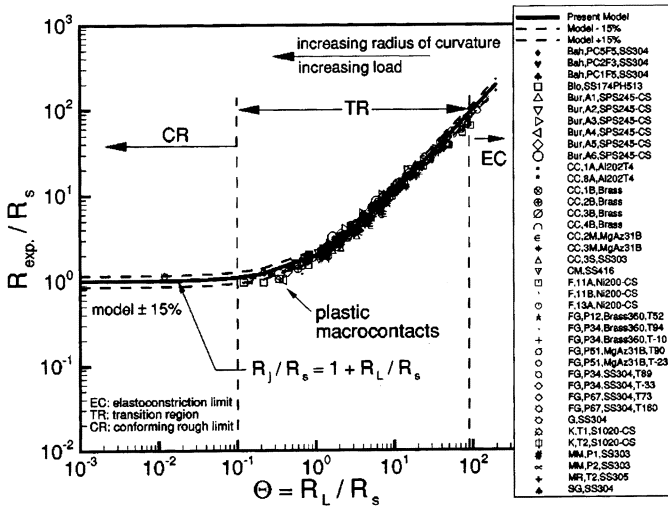


Fig. 33. Comparison of compact model with all conforming and nonconforming rough surface data.

to the elastoconstriction (EC) model when $\Theta \geq 100$, and it approaches the conforming rough surface (CR) model when $\Theta \leq 0.10$ which are the two asymptotes. The transition from the CR model to the EC model occurs when $0.10 \leq \Theta \leq 100$.

The comparison of the compact model predictions and all vacuum data for conforming rough surfaces are shown in Fig. 32. All data fall well within the $\pm 15\%$ bounds.

Fig. 33 shows the comparison of the compact model with all vacuum data obtained for conforming and nonconforming rough surfaces. In this plot the dimensionless experimental joint resistance values defined as R_{exp}/R_p are plotted against the theoretical model given as $0.36/P^* + 4 = R_L/R_p L(1 - a_L/b_L)^{1.5}/a_L$. The comparison is made over five decades. With the exception of the data denoted as “truncation effect”, all data fall within the $\pm 15\%$ bounds. The experimental data include several metals and alloys, 75 data sets, more than 880 test points collected by many researchers during the past 40 years that cover a wide range of micro and macro surface parameters.

The comparisons demonstrate the validity and accuracy of the compact model which show an RMS difference of about 13.8% with all data.

VIII. FUTURE RESEARCH DIRECTIONS

The geometric-mechanical-thermal models developed for conforming rough gaussian surfaces (e.g., bead blasted) should be extended to include nongaussian surface roughness which is generated by machining processes such as grinding, milling, turning, fly-cutting, etc. The effect of asperity height truncation which was observed at low apparent contact pressures with the very rough surfaces should be examined both analytically and experimentally. As contact pressures decrease well below atmospheric pressure levels, the truncation effects on contact and microgap conductances will become more important for the microelectronics industry.

For joints formed by very smooth surfaces at very light contact pressures, it will be necessary to measure accurately the surface roughness parameters and the microhardness measurements will require novel instruments such as nano-indenters. The contact microhardness may be quite different from the values which have been measured and correlated to date.

Thin polymeric materials are frequently employed as inserts between rough metal surfaces. This will require an examination and re-evaluation of the thermomechanical models which are available for metal-metal joints. The thermophysical properties of the polymeric materials should be measured and quantified.

The use of TIMs for microelectronic applications will require extensive experimental research to measure and quantify their thermal properties as well as their rheological characteristics when placed between two rough metal surfaces which are mechanically loaded. There are many types of TIMs. Some are simple mixtures of a substance called the matrix which is filled with many small sized solid particles having thermal conductivities much greater than the matrix. Increasing the volume fraction of the filler increases the effective thermal conductivity as well as the effective viscosity which prevents the movement of the TIM in the microgaps. Some TIMs consist of a thin metallic carrier such as Aluminum foil which is coated on one or both sides with a thin layer of low thermal conductivity paraffin which may or may not be filled with micron sized solid particles to increase the thermal conductivity of the paraffin. Extensive thermal tests are required to characterized these TIMS before simple models can be developed.

IX. CONCLUSION

The paper highlights some of the TCR research done since 1963. The research which began at MIT, Cambridge, MA from 1963 to 1967, and Poitiers, France from 1967 to 1969, has continued since 1970 at the University of Waterloo in Canada. The theoretical and experimental research on thermal contact resistance of conforming rough surfaces has occupied many graduate students since 1970.

The thermal and geometric parts of the TCR problem which appeared in the original CMY model were developed for gaussian surface roughness. They have remained unchanged; however, the mechanical part has undergone several modifications and extensions over the past four decades. First, the microhardness layer, determined by Vickers microhardness measurements of several metals, was correlated and incorporated into the mechanical part of the TCR model. Subsequently an explicit relation was developed that showed that contact

microhardness was dependent on material properties, surface roughness parameters, and apparent contact pressure. Later the Vickers microhardness coefficients were correlated with Brinell hardness. The modified CMY model was extended to include the effect of soft, high thermal conductivity layers such as silver.

A statistical microgap conductance model was developed that incorporates the effects of contact pressure and gas pressure through the gas rarefaction parameters. Several gases such as argon, nitrogen, and helium were used in joints formed by different metals having a wide range of surface roughness to validate the gap and joint conductance models.

Thermomechanical models were developed for the elastoconstriction resistance and elastogap resistance of nonconforming smooth surfaces such as sphere-flat contacts. The models were validated by extensive experiments with various gases in the macrogap at gas pressures ranging from atmospheric to near vacuum.

Elastoplastic contact models were developed for the smooth nonconforming solids such as a sphere-flat contact, and the conforming rough surface joint. These mechanical models were incorporated into the thermal joint resistance and thermal joint contact conductance models. The elastoplastic contact models were validated by experiments.

A thermomechanical model was developed to account for mechanical and thermal effects of thin layers (coatings) on the elastoconstriction of sphere-flat contacts.

A simple model was developed for TIMs such as oil, greases, greases filled with solid particles, and phase change materials. The model was compared with recently published data and showed similar trends and values of joint resistance. The agreement between data and model predictions was best when the surface roughness was large (large microgaps) and the grease was filled with small sized particles and the volume fraction was low.

ACKNOWLEDGMENT

The author wishes to thank Dr. M. Bahrami, University of Waterloo, for his assistance in the preparation of this paper, and the ITherm 2004 Achievement Award Committee and Program Committee, for inviting him to submit this Keynote Paper.

REFERENCES

- [1] T. R. Thomas and S. D. Probert, "Thermal contact of solids," *Chem. Process Eng.*, pp. 1–12, Nov. 1966.
- [2] M. M. Yovanovich and H. Fenech, "Thermal contact conductance of nominally flat rough surfaces in a vacuum environment," in *Thermophysics and Temperature Control of Spacecraft and Entry Vehicles*, G. B. Heller, Ed. New York: Academic, 1966, vol. 18, pp. 773–794.
- [3] M. M. Yovanovich, "Thermal contact resistance across elastically deformed spheres," *J. Spacecraft Rockets*, vol. 4, pp. 119–121, 1967.
- [4] M. M. Yovanovich, H. Cordier, and J. Coutanceau, "Sur la resistance thermique due a un contact unique de section circulaire," *C.R. Acad. Sci. Paris*, vol. t. 268, pp. 1–4, Jan. 1969.
- [5] M. G. Cooper, B. B. Mikic, and M. M. Yovanovich, "Thermal contact conductance," *Int. J. Heat Mass Transf.*, vol. 12, pp. 279–300, 1969.
- [6] M. M. Yovanovich, "Overall constriction resistance between contacting rough, wavy surfaces," *Int. J. Heat Mass Transf.*, vol. 12, pp. 1517–1520, 1969.
- [7] M. M. Yovanovich and M. Tuarze, "Experimental evidence of thermal resistance at soldered joints," *J. Spacecraft Rockets*, vol. 6, no. 7, pp. 855–857, 1969.
- [8] M. M. Yovanovich, "A correlation of the minimum thermal resistance of soldered joints," *J. Spacecraft Rockets*, vol. 7, no. 8, pp. 1013–1014, 1970.
- [9] —, "Thermal constriction resistance between contacting metallic paraboloids: application to instrument bearings," in *Proc. 5th AIAA Thermophysics Conf.*, Los Angeles, CA, June 29–July 1 1971.
- [10] —, "Thermal conductance of turned surfaces," in *Proc. 9th Aerospace Sciences Meeting*, Los Angeles, CA, Jan. 25–27, 1971.
- [11] —, "Thermal conductance of a row of cylinders contacting two planes," in *Proc. AIAA 6th Thermophysics Conf.*, Tullahoma, TN, Apr. 26–28, 1971.
- [12] V. S. Cecco and M. M. Yovanovich, "Electrical measurement of joint resistance at perfect contact interfaces: application to thermal joint conductance," in *Proc. AIAA 10th Aerospace Sciences Meeting*, San Diego, CA, Jan. 17–19, 1972.
- [13] M. M. Yovanovich, "Investigation on the effect of metallic foils upon thermal joint resistance: evidence of optimum foil thickness," in *Proc. AIAA 7th Thermophysics Conf.*, San Antonio, TX, Apr. 10–12, 1973.
- [14] M. M. Yovanovich and W. W. Kitscha, "Modeling the effect of air and oil upon the thermal resistance of a sphere-flat contact," in *Proc. AIAA 8th Thermophysics Conf.*, Palm Springs, CA, Jul. 16–18, 1973.
- [15] G. E. Schneider and M. M. Yovanovich, "Correlation of the over-all thermal resistance of metallic O-rings contacting two cylinders," *J. Spacecraft Rockets*, vol. 11, no. 3, pp. 206–208, Mar. 1974.
- [16] A. B. Strong, G. E. Schneider, and M. M. Yovanovich, "Thermal constriction resistance of a disk with arbitrary heat flux—finite difference solution in oblate spheroidal coordinates," in *Proc. AIAA/ASME'74 Conf.*, Boston, MA, 1974.
- [17] W. W. Kitscha and M. M. Yovanovich, "Experimental investigation on the overall thermal resistance of sphere-flat contacts," in *Proc. AIAA 12th Aerospace Sciences Meeting*, Washington, DC, Jan. 30–Feb. 1 1974.
- [18] S. Cividino, M. M. Yovanovich, and L. S. Fletcher, "A model for predicting the joint conductance of a woven wire screen contacting two solids," in *Proc. AIAA/ASME'74 Thermophysics Heat Transfer Conf.*, Boston, MA, Jul. 15–17, 1975.
- [19] G. E. Schneider, A. B. Strong, and M. M. Yovanovich, "Transient heat flow from a thin circular disk," in *Proc. AIAA 10th Thermophysics Conf.*, Denver, CO, May 27–29, 1975.
- [20] M. M. Yovanovich, "General thermal constriction parameter for annular contacts on circular flux tubes," *AIAA J.*, vol. 14, no. 6, pp. 822–824, 1976.
- [21] M. M. Yovanovich, "General expressions for constriction resistance due to arbitrary flux distributions at nonsymmetric, coaxial contacts," in *Proc. 13th Aerospace Sciences Meeting*, Pasadena, CA, Jan. 20–22, 1976.
- [22] —, "Thermal constriction resistance of contacts on a half-space: integral formulation," in *Proc. AIAA 10th Thermophysics Conf.*, Denver, CO, May 27–29, 1976.
- [23] M. M. Yovanovich, S. S. Burde, and J. C. Thompson, "Thermal constriction resistance of arbitrary planar contacts with constant flux," in *Proc. AIAA 11th Thermophysics Conf.*, San Diego, CA, Jul. 14–16, 1977.
- [24] G. E. Schneider, A. B. Strong, and M. M. Yovanovich, "Transient thermal response to two bodies communicating through a small circular contact area," *Int. J. Heat Mass Transf.*, vol. 20, pp. 301–308, 1977.
- [25] M. M. Yovanovich and S. S. Burde, "Centroidal and area average resistances of nonsymmetric, singly connected contacts," *AIAA J.*, vol. 15, no. 10, pp. 1523–1525, 1977.
- [26] M. M. Yovanovich, "Simplified explicit elastoconstriction resistance expression for ball/race contacts," in *Proc. AIAA 16th Aerospace Sciences Meeting*, Huntsville, AL, Jan. 16–18, 1978.
- [27] M. M. Yovanovich and S. S. Burde, "Thermal resistance at smooth sphere/rough flat contacts—theoretical analysis," in *Proc. 2nd AIAA/ASME Thermophysics Heat Transfer Conf.*, Palo Alto, CA, May 24–27, 1978.
- [28] S. S. Burde and M. M. Yovanovich, "Thermal resistance at smooth sphere/rough flat contacts," *AIAA Progress Astronaut. Aeronaut.*, vol. 65, pp. 83–102, 1979.
- [29] M. M. Yovanovich, K. A. Martin, and G. E. Schneider, "Constriction resistance of doubly-connected contact area under uniform flux," in *Proc. AIAA 14th Thermophysics Conf.*, Orlando, FL, Jun. 4–6, 1979.
- [30] M. M. Yovanovich, G. E. Schneider, and V. S. Cecco, "Electrical interface resistance and potential field mapping of explosive bonded interfaces," in *Proc. AIAA 18th Aerospace Sciences Meeting*, Pasadena, CA, Jan. 14–16, 1980.
- [31] M. M. Yovanovich, "New contact and gap conductance correlations for conforming rough surfaces," in *Proc. AIAA 16th Thermophysics Conf.*, Palo Alto, CA, Jun. 23–25, 1981.

- [32] M. M. Yovanovich, A. Hegazy, and J. DeVaal, "Surface hardness distribution effects upon contact, gap and joint conductances," in *Proc. AIAA/ASME 3rd Joint Thermophysics, Fluids, Plasma Heat Transfer Conf.*, St. Louis, MO, Jun. 7–11, 1982.
- [33] M. M. Yovanovich, J. DeVaal, and A. Hegazy, "A statistical model to predict thermal gap conductance between conforming rough surfaces," in *Proc. AIAA/ASME 3rd Joint Thermophysics, Fluids, Plasma Heat Transfer Conf.*, St. Louis, MO, Jun. 7–11, 1982.
- [34] M. H. Schankula, D. W. Patterson, and M. M. Yovanovich, "The effect of oxide films on the thermal resistance between contacting zirconium alloys," in *Proc. Materials Nuclear Energy Conf.*, Huntsville, ON, Canada, Sep. 29–Oct. 2 1983, pp. 106–111.
- [35] M. M. Yovanovich and A. Hegazy, "An accurate universal contact conductance correlation for conforming rough surfaces with different micro-hardness profiles," in *Proc. AIAA 18th Thermophysics Conf.*, Montreal, QC, Canada, Jun. 1–3, 1983.
- [36] M. M. Yovanovich, N. J. Fisher, and H. J. Saabas, "A light load model combining surface roughness and waviness to predict thermal contact conductance," in *Proc. AIAA 18th Thermophysics Conf.*, Montreal, QC, Canada, Jun. 1–3, 1983.
- [37] M. M. Yovanovich, J. C. Thompson, and K. J. Negus, "Thermal resistance of arbitrarily shaped contacts," in *Proc. 3rd Int. Conf. Numerical Methods Thermal Problems*, R. W. Lewis, J. A. Johnson, and R. Smith, Eds., Seattle, WA, Aug. 2–5, 1983, pp. 1072–1082.
- [38] V. W. Antonetti and M. M. Yovanovich, "Using metallic coatings to enhance thermal contact conductance of electronic packages," *Proc. 1983 ASME Winter Annu. Meeting*, pp. 59–69, Nov. 13–18, 1983.
- [39] M. M. Yovanovich, K. J. Negus, and J. C. Thompson, "Transient temperature rise of arbitrary contacts with uniform flux by surface element methods," in *Proc. AIAA 22nd Aerospace Sciences Meeting*, Reno, NV, Jan. 9–12, 1984.
- [40] K. A. Martin, M. M. Yovanovich, and Y. L. Chow, "Method of moments formulation of thermal constriction resistance of arbitrary contacts," in *Proc. AIAA 19th Thermophysics Conf.*, Snowmass, CO, Jun. 25–28, 1984.
- [41] B. J. Rozon, P. F. Galpin, G. E. Schneider, and M. M. Yovanovich, "The effect of geometry on the contact conductance of contiguous interfaces," in *Proc. AIAA 19th Thermophysics Conf.*, Snowmass, CO, Jun. 25–28, 1984.
- [42] K. A. Martin, M. M. Yovanovich, and Y. L. Chow, "Method of moments formulation of thermal constriction resistance of arbitrary contacts," in *Proc. AIAA 19th Thermophysics Conf.*, Snowmass, CO, Jun. 1984.
- [43] P. J. Turyk and M. M. Yovanovich, "Transient constriction resistance for elemental flux channels heated by uniform flux sources," in *Proc. ASME/AICHE National Heat Transfer Conf.*, Niagara Falls, NY, Aug. 6–8, 1984.
- [44] V. W. Antonetti and M. M. Yovanovich, "Enhancement of thermal contact conductance by metallic coatings: theory and experiment," *ASME J. Heat Transf.*, vol. 107, pp. 513–519, Aug. 1984.
- [45] M. M. Yovanovich, G. R. McGee, and M. H. Schankula, "Ellipsoidal thermal constriction model for crowned-cylinder/flat elastic contacts," in *Proc. 22nd ASME/AICHE Nat. Heat Transfer Conf.*, Niagara Falls, NY, Aug. 6–8, 1984.
- [46] K. J. Negus and M. M. Yovanovich, "Constriction resistance of circular flux tubes with mixed boundary conditions by linear superposition of neumann solutions," in *Proc. 22nd ASME/AICHE Nat. Heat Transfer Conf.*, Niagara Falls, NY, Aug. 6–8, 1984.
- [47] —, "Application of the method of optimized images to steady three-dimensional conduction problems," in *Proc. ASME WAM Meeting*, New Orleans, LA, Dec. 9–13, 1984.
- [48] H. J. Saabas, N. J. Fisher, and M. M. Yovanovich, "Circular and annular constriction resistances within a compound thermal spreader for cooling microelectronic devices," in *Proc. AIAA 23rd Aerospace Sciences Meeting*, Reno, NV, Jan. 14–17, 1985.
- [49] K. J. Negus, M. M. Yovanovich, and J. W. DeVaal, "Development of thermal constriction resistance for anisotropic rough surfaces by the method of infinite images," in *Proc. 23rd ASME-AICHE Nat. Heat Transfer Conf.*, Denver, CO, Aug. 4–7, 1985.
- [50] H. J. Saabas and M. M. Yovanovich, "Application of SEM and superposition techniques to circular microcontacts distributed over elliptical contours on circular flux tubes and half-spaces," in *Proc. AIAA 20th Thermophysics Conf.*, Williamsburg, VA, Jun. 19–21, 1985.
- [51] G. R. McGee, M. H. Schankula, and M. M. Yovanovich, "Thermal resistance of cylinder-flat contacts: theoretical analysis and experimental verification of a line contact model," *Nucl. Eng. Design*, vol. 86, pp. 369–381, 1985.
- [52] J. Dryden, M. M. Yovanovich, and A. S. Deakin, "The effect of coatings upon the steady-state and short time constriction resistance for an arbitrary axisymmetric flux," *ASME J. Heat Transf.*, vol. 107, pp. 33–38, Feb. 1985.
- [53] D. A. Wesley and M. M. Yovanovich, "A new gaseous gap conductance relationship," *Nucl. Technol.*, vol. 72, pp. 70–74, 1986.
- [54] N. J. Fisher and M. M. Yovanovich, "Thermal constriction resistance of sphere/layered flat contacts: theory and experiment," in *Proc. 4th ASME/AIAA Thermophysics Heat Transfer Conf.*, Boston, MA, Jun. 1–4, 1986, pp. 219–229.
- [55] K. J. Negus, C. A. Vanoverbeke, and M. M. Yovanovich, "Thermal resistance of a bolted microelectronic chip carrier: effect of contact conductance," in *Proc. 22nd AIAA Thermophysics Conf.*, Honolulu, HI, Jun. 8–10, 1987.
- [56] C. A. Vanoverbeke, K. J. Negus, and M. M. Yovanovich, "Thermal constriction resistance with variable conductivity near the contact surface," in *Proc. 24th Nat. Heat Transfer Conf.*, Pittsburg, PA, Aug. 9–12, 1987, pp. 91–98.
- [57] J. W. DeVaal and M. M. Yovanovich, "The effects of surface slope anisotropy on the contact conductance of conforming rough surfaces," in *Proc. 24th Nat. Heat Transfer Conf.*, Pittsburgh, PA, Aug. 9–12, 1987, pp. 123–134.
- [58] K. J. Negus and M. M. Yovanovich, "Simple separability for steady heat conduction with spatially-varying thermal conductivity," *Int. J. Heat Mass Transf.*, Jul. 1986.
- [59] M. M. Yovanovich, "Recent developments in thermal contact, gap and joint conductance theories and experiment," in *Proc. Keynote Paper Int. Heat Transfer Conf.*, San Francisco, CA, Aug. 17–22, 1986.
- [60] T. F. Lemczyk and M. M. Yovanovich, "New models and methodology for predicting thermal contact resistance in compound cylinders and fin-tubes," in *Proc. Thermal/Mechanical Heat Exchanger Design—Karl Gardner Memorial Session*, Anaheim, CA, Dec. 7–12, 1987, pp. 59–70.
- [61] K. J. Negus, M. M. Yovanovich, and J. C. Thompson, "Constriction resistance of circular contacts on coated surfaces: effect of contact boundary conditions," *J. Thermophys. Heat Transf.*, vol. 2, no. 2, pp. 158–164, 1988.
- [62] K. J. Negus and M. M. Yovanovich, "Correlation of gap conductance integral for conforming rough surfaces," *J. Thermophys. Heat Transf.*, vol. 2, no. 3, pp. 279–281, 1988.
- [63] S. Song and M. M. Yovanovich, "Relative contact pressure: dependence upon surface roughness and vickers microhardness," *J. Thermophys. Heat Transf.*, vol. 2, no. 1, pp. 43–47, 1988.
- [64] M. M. Yovanovich, "Fundamentals of thermal constriction (spreading) resistance for electronic cooling," in *Proc. 20th Int. Symp. Heat Transfer Electron. Microelectron. Equipment*, Dubrovnik, Yugoslavia, Aug. 29–Sep. 2 1988.
- [65] T. F. Lemczyk and M. M. Yovanovich, "Thermal constriction resistance with convective boundary conditions, part 1: half-space contacts; part 2: layered half-space contacts," *Int. J. Heat Mass Transf.*, vol. 31, no. 9, pp. 1861–1872, 1988.
- [66] —, "Thermal constriction resistance with convective boundary conditions, part 2: layered half-space contacts," *Int. J. Heat Mass Transf.*, vol. 31, no. 9, pp. 1873–1883, 1988.
- [67] M. M. Yovanovich and V. W. Antonetti, "Application of thermal contact resistance theory to electronic packages," in *Advances in Thermal Modeling of Electronic Components and Systems*, A. Bar-Cohen and A. D. Kraus, Eds. New York: Hemisphere, 1988, vol. 1, ch. 2, pp. 79–128.
- [68] N. J. Fisher and M. M. Yovanovich, "Thermal constriction resistance of sphere/layered flat contacts: theory and experiments," *J. Heat Transf.*, vol. 111, pp. 249–256, May 1989.
- [69] K. J. Negus, M. M. Yovanovich, and J. V. Beck, "On the non-dimensionalization of constriction resistance for semi-infinite heat flux tubes," *J. Heat Transf.*, vol. 111, pp. 804–807, Aug. 1989.
- [70] K. M. Nho and M. M. Yovanovich, "Measurement of contact resistance in finned tube heat exchangers," in *Proc. ASHRAE Winter Meeting*, Chicago, IL, Jan. 30–Feb. 1 1989.
- [71] —, "Effect of oxide layers on measured and theoretical contact conductances in finned—tube exchangers," in *Proc. A.L. London Symp.*, Stanford, CA, Mar. 23–24, 1989.
- [72] M. M. Yovanovich and K. M. Nho, "Experimental investigation of heat flow rate and direction on contact resistance of ground/lapped stainless/steel interfaces," in *Proc. AIAA 24th Thermophysics Conf.*, Buffalo, NY, Jun. 12–15, 1989.
- [73] S. Song and M. M. Yovanovich, "Contact interface gas heat transfer: a method of measuring thermal accommodation coefficient," in *Proc. 9th Annu. Int. Electronics Packaging Conf.*, vol. 2, Sep. 10–14, 1989, pp. 925–936.

- [74] S. Song, M. M. Yovanovich, and K. Nho, "Thermal gap conductance: effect of gas pressure and mechanical load," *J. Thermophys. Heat Transf.*, vol. 6, no. 1, pp. 62–68, 1992.
- [75] S. Song, M. M. Yovanovich, and F. O. Goodman, "Thermal gap conductance of conforming surfaces in contact," *ASME J. Heat Transf.*, vol. 115, pp. 533–540, 1993.
- [76] S. Lee, M. M. Yovanovich, S. Song, and K. P. Moran, "Analysis of thermal constriction resistance in bolted joints," *Int. J. Microcirc. Electron. Packag.*, vol. 16, no. 2, pp. 125–136, 1993.
- [77] M. H. Attia and M. M. Yovanovich, "A model for predicting the thermal constriction resistance in fretting," in *Proc. 114th ASME Winter Annu. Meeting*, New Orleans, LA, Nov. 28–Dec. 3 1993.
- [78] M. R. Sridhar and M. M. Yovanovich, "Review of elastic and plastic contact conductance models: comparison with experiment," *J. Thermophys. Heat Transf.*, vol. 8, no. 4, pp. 633–640, 1994.
- [79] M. B. H. Mantelli and M. M. Yovanovich, "Experimental determination of overall thermal resistance of satellite bolted joints," in *32nd Aerospace Sciences Meeting & Exhibit*, Reno, NV, Jan. 10–13, 1994.
- [80] M. M. Yovanovich, "Constriction resistance of planar isoflux heat sources within semi-infinite conductors: image method," in *Proc. 4th ASME/JSME Thermal Engineering Joint Conf.*, Maui, HI, Mar. 19–24, 1995.
- [81] M. R. Sridhar and M. M. Yovanovich, "Elastoplastic constriction resistance of sphere-flat contacts: theory and experiment," *ASME J. Heat Transf.*, vol. 118, no. 1, pp. 202–205, 1996.
- [82] —, "Thermal contact conductance of tool steel and comparison with model," *Int. J. Heat Mass Transf.*, vol. 39, no. 4, p. 831, 1996.
- [83] —, "Empirical methods to predict vickers microhardness," *WEAR*, vol. 193, no. 1, pp. 91–98, 1996.
- [84] —, "Elastoplastic contact conductance model for isotropic conforming rough surfaces and comparison with experiments," *ASME J. Heat Transf.*, vol. 118, no. 1, pp. 3–9, 1996.
- [85] M. B. H. Mantelli and M. M. Yovanovich, "Experimental determination of the overall thermal resistance of satellite bolted joints," *J. Thermophys. Heat Transf.*, vol. 10, no. 1, pp. 177–179, 1996.
- [86] Y. S. Muzychka, M. R. Sridhar, M. M. Yovanovich, and V. W. Antonetti, "Thermal constriction resistance in multilayered contacts: applications in thermal contact resistance," in *Proc. Thermophysics Thermophysical Properties Session, 1996 AIAA Nat. Heat Transfer Conf.*, Houston, TX, Aug. 3–6, 1996.
- [87] M. M. Yovanovich, "Transient spreading resistance of arbitrary isoflux contact areas: development of a universal time function," in *Proc. AIAA 32nd Thermophysics Conf.*, Atlanta, GA, Jun. 23–25, 1997.
- [88] M. B. H. Mantelli and M. M. Yovanovich, "Parametric heat transfer study of bolted joints," *J. Thermophys. Heat Transf.*, vol. 12, no. 3, pp. 382–390, 1998.
- [89] M. M. Yovanovich, J. R. Culham, and P. Teertstra, "Analytical modeling of spreading resistance in flux tubes, half spaces, and compound disks," *IEEE Trans. Compon., Packag. Manufact. Technol. A*, vol. 21, no. 1, pp. 168–176, Mar. 1998.
- [90] M. B. H. Mantelli and M. M. Yovanovich, "Compact analytical model for overall thermal resistance of bolted joints," *Int. J. Heat Mass Transf.*, vol. 41, no. 10, pp. 1255–1266, 1998.
- [91] M. M. Yovanovich, Y. S. Muzychka, and J. R. Culham, "Spreading resistance in isoflux rectangles and strips on compound flux channels," *J. Thermophys. Heat Transf.*, vol. 13, no. 4, pp. 495–500, 1999.
- [92] M. Stevanović and M. M. Yovanovich, "Modeling thermal constriction resistance of sphere-layered substrate in elastic contact," in *Proc. 37th AIAA Aerospace Sciences Meeting Exhibit*, Reno, NV, Jan. 11–14, 1999.
- [93] M. M. Yovanovich, "Thermal-mechanical models for nonconforming surface contacts," in *Itherm 2000 Proc. 7th Intersoc. Conf. Thermal Thermomechanical Phenomena Electronics Systems*, vol. 1, Las Vegas, NV, May 25–28, 2000.
- [94] J. R. Culham, P. Teertstra, and M. M. Yovanovich, "The role of spreading resistance on effective conductivity in laminated substrates," *Future Circuits*, vol. 6, pp. 73–78, 2000.
- [95] Y. S. Muzychka, M. Stevanović, and M. M. Yovanovich, "Thermal spreading resistance in compound annular sectors," *AIAA J. Thermophys. Heat Transf.*, vol. 15, no. 2, pp. 354–359, 2001.
- [96] M. Stevanović, M. M. Yovanovich, and J. R. Culham, "Modeling contact between rigid sphere and elastic layer bonded to rigid substrate," *IEEE Trans. Compon. Packag. Technol.*, vol. 24, no. 2, pp. 207–212, 2001.
- [97] Y. S. Muzychka, M. M. Yovanovich, and J. R. Culham, "Applications of thermal spreading resistance in compound and orthotropic systems," in *Proc. 39th Aerospace Sciences Meeting Exhibit*, Reno, NV, Jan. 8–11, 2001.
- [98] I. Savija, M. M. Yovanovich, J. R. Culham, and E. E. Marotta, "Review of thermal conductance models for joints incorporating enhancement materials," *J. Thermophys. Heat Transf.*, vol. 17, no. 1, pp. 43–52, 2003.
- [99] —, "Thermal joint resistance of conforming rough surfaces with grease-filled interstitial gaps," *J. Thermophys. Heat Transf.*, vol. 17, no. 1, pp. 278–282, 2003.
- [100] I. Savija, J. R. Culham, and M. M. Yovanovich, "Effective thermophysical properties of thermal interface materials: part I definitions and models," in *Proc. Int. Electronic Packaging Technical Conf. Exhibit*, Maui, HI, Jul. 6–11, 2003.
- [101] —, "Effective thermophysical properties of thermal interface materials: part II experiments and data," in *Proc. Int. Electronic Packaging Technical Conf. Exhibit*, Maui, HI, Jul. 6–11, 2003.
- [102] F. H. Milanez, M. M. Yovanovich, and J. R. Culham, "Effect of surface asperity truncation on thermal contact conductance," *IEEE Trans. Compon. Packag. Technol.*, vol. 26, no. 1, pp. 48–54, Mar. 2003.
- [103] F. H. Milanez, J. R. Culham, and M. M. Yovanovich, "Experimental thermal contact conductance of bead-blasted SS 304 at light loads," *J. Thermophys. Heat Transf.*, vol. 17, no. 4, pp. 534–542, 2003.
- [104] M. B. H. Mantelli and M. M. Yovanovich, "Thermal contact resistance," in *Spacecraft Thermal Control Handbook*, 2nd ed., D. G. Gilmore, Ed. El Segundo, CA: Aerospace, 2003, vol. 1, pp. 599–637.
- [105] M. M. Yovanovich and E. E. Marotta, "Thermal spreading and contact resistances," in *Heat Transfer Handbook*, A. Bejan and A. D. Kraus, Eds. New York: Wiley, 2003, ch. 4, pp. 261–393.
- [106] M. M. Yovanovich, "Thermal resistances of circular source on finite circular cylinder with side and end cooling," *ASME J. Electron. Packag.*, vol. 125, no. 2, pp. 169–177, 2003.
- [107] Y. S. Muzychka, J. R. Culham, and M. M. Yovanovich, "Thermal spreading resistance of eccentric heat sources on rectangular flux channels," *ASME J. Electron. Packag.*, vol. 125, no. 2, pp. 178–185, 2003.
- [108] M. Bahrami, J. R. Culham, M. M. Yovanovich, and G. E. Schneider, "Review of thermal joint resistance models for nonconforming rough surfaces," *Appl. Mech. Rev. J.*, to be published.
- [109] —, "Modeling thermal contact resistance: a scale analysis approach," *ASME J. Heat Transf.*, vol. 126, pp. 896–905, 2004.
- [110] M. Bahrami, M. M. Yovanovich, and J. R. Culham, "A compact model for contact of rough spheres," *J. Tribology*, to be published.
- [111] M. Bahrami, J. R. Culham, M. M. Yovanovich, and G. E. Schneider, "Thermal contact resistance of nonconforming rough surfaces, part 1: contact mechanics model," *J. Thermophys. Heat Transf.*, vol. 18, no. 2, pp. 209–217, 2004.
- [112] —, "Thermal contact resistance of nonconforming rough surfaces, part 2: thermal model," *J. Thermophys. Heat Transf.*, vol. 18, no. 2, pp. 218–227, 2004.
- [113] M. Bahrami, M. M. Yovanovich, and J. R. Culham, "Thermal joint resistances of conforming rough surfaces with gas-filled gaps," *J. Thermophys. Heat Transf.*, vol. 18, no. 3, pp. 318–325, 2004.
- [114] —, "Thermal joint resistances of nonconforming rough surfaces with gas-filled gaps," *J. Thermophys. Heat Transf.*, vol. 18, no. 3, pp. 326–332, 2004.



M. Michael Yovanovich received the Sc.D. degree from the Massachusetts Institute of Technology, Cambridge.

He is a Distinguished Professor Emeritus of mechanical engineering at the University of Waterloo, Waterloo, ON, Canada, and is the Principal Scientific Advisor to the Microelectronics Heat Transfer Laboratory. He has published more than 350 journal and conference papers, and numerous technical reports, as well as three chapters in handbooks on conduction and thermal contact resistance. He has been a consultant to several North American nuclear, aerospace, and microelectronics industries and national laboratories. His research in the field of thermal modeling includes analysis of complex heat conduction problems, external and internal natural and forced convection heat transfer from and in complex geometries, and contact resistance theory and applications.

Dr. Yovanovich received the AIAA Thermophysics Award and the ASME Heat Transfer Award. He is a Fellow of AAAS, AIAA, and ASME.